ELSEVIER

Precambrian Research 118 (2002) 59–82

Precambrian Research

www.elsevier.com/locate/precamres

A late Neoproterozoic magmatic core complex in the Eastern Desert of Egypt: emplacement of granitoids in a wrench-tectonic setting

M. Bregar [a], A. Bauernhofer [a], K. Pelz [b], U. Kloetzli [c], H. Fritz [a,*], P. Neumayr [d]

[a] *Institut für Geologie und Paläontologie, Karl-Franzens Universität Graz, Heinrichstrasse 26, A-8010 Graz, Austria*
[b] *GeoForschungsZentrum Potsdam, Telegrafenberg C228, Potsdam, Germany*
[c] *Laboratorium für Geochronologie, Institut für Geologie, Universität Wien, Wien, Austria*
[d] *Department of Geology and Geophysics, Centre for Strategic Mineral Deposits, The University of Western Australia, Nedlands, Australia*

Received 5 July 1999; accepted 2 May 2002

Abstract

Core complexes within the Eastern Desert of Egypt evolved in the course of orogen-parallel extension during Neoproterozoic plate convergence. In the Sibai Core complex, more than 90% of the exposed surface consists of magmatic rocks. In this study four magmatic suites have been distinguished. They are geochemically characterised and their intrusion ages are determined using the Pb/Pb single zircon evaporation technique. Results show that all magmatic suites formed during Neoproterozoic tectonics. The oldest, calc-alkaline rocks of group (I) gave ages of 670–690 Ma and are related to subduction processes in an island-arc setting. Subsequent orogen-parallel extension was accompanied by the intrusion of group (II) and (III) granitoids yielding ages of 655 and 645 Ma, respectively. The younger, felsic granites of group (IV) intruded along pre-existing structures and exhibit variable composition. We relate emplacement of various granitoids within the Sibai to progressively evolving structures. Group (I) represents the deep level of an island arc and exhibits nappe stacking structures related to oblique convergence in the late Neoproterozoic. Group (II) granitoids have been emplaced at mid-crustal levels and portray transpression and orogen-parallel extrusion dynamics. Related structures are represented by an older set of sinistral shear zones. Granitoids of group (III) intruded upper crustal levels during exhumation of the Sibai Core complex. Their emplacement was controlled by the pull-apart regime of a younger set of sinistral shear zones and associated normal shear zones. Denudation due to ongoing orogen-parallel extension is evident from deposition of sediments within the adjacent intramontane Kareim molasse basin. The sediments were intruded by post-tectonic granitoids of group (IV). Close relations between core complex formation and ongoing magmatic activity define the Sibai as a magmatic core complex.

* Corresponding author. Fax: +43-316-380-9870
E-mail address: harald.fritz@kfunigraz.ac.at (H. Fritz).

0301-9268/02/$ - see front matter
PII: S0301-9268(02)00062-1

Keywords: Egypt; East African Orogen; Neoproterozoic; Exhumation; Core complexes; Granites

1. Introduction

It is widely accepted that the East African Orogen in the Eastern Desert of Egypt consolidated in the Neoproterozoic by accretion of island arcs (e.g. Gass, 1982; Stern, 1994; Kröner et al., 1994). In this convergent tectonic environment, large amount of ophiolites and related sedimentary strata has been obducted. Structural basement units beneath obducted remnants of oceanic lithosphere are exposed within core complexes (Sturchio et al., 1983; Fritz et al., 1996; Fowler and Osman, 2001). These consist of magmatic or metamorphic rocks tectonically separated from the cover units. Similar core complexes have also been reported from the Wadi Kid area in the Sinai (El Gaby et al., 1991; Blasband et al., 1997, 2000). The core complexes in the Central Eastern Desert are aligned NW–SE which is roughly parallel to the overall strike of the orogen and parallel to the strike of the Najd Fault System (Stern, 1985; Fritz et al., 1996). The nature and origin of these core complexes are a matter of intense discussion. Based on structural arguments and the succession of magmatic events, a pre-Neoproterozoic age has been proposed for these units (Sturchio et al., 1983; El Gaby et al., 1990; Khudeir et al., 1995). However, available geochronological data of thermal events within these basement rocks cluster around two peaks at 750 and 600 Ma (Stern and Hedge, 1985; Kröner et al., 1994), whereas the existence of older crust is poorly constrained.

This work focuses on the tectonothermal evolution of the structural basement exposed in the Sibai magmatic core complex (Fig. 1). The basement consists almost entirely of granitoids and is separated from the structural cover by strike-slip and extensional shear zones. A combined kinematic, geochemical and geochronological approach using Pb/Pb single zircon ages (evaporation technique) is used to relate magmatism and deformation to exhumation of the Sibai magmatic core complex. It will be shown that large amount of juvenile crust formed during Neoproterozoic convergence that was simultaneously deformed by wrench tectonics. Furthermore we show how magma generation was related to overall oblique convergence and subsequent orogen-parallel extension along a wrench corridor in the Sibai.

A second aspect of this paper, involving geochemical investigations, is to specify the geotectonic setting of the wrench tectonism responsible for the exhumation of core complexes in the Eastern Desert, The lithosphere within the Eastern Desert experienced minor thickening as a consequence of oblique island arc accretion and coeval orogen-parallel wrench tectonics (Stern, 1994; Fritz et al., 1996, 2002; Neumayr et al., 1998). Hence, buoyancy driven mechanisms usually proposed for collisional orogens arc not suitable to explain exhumation of core complexes in this area. An alternative view is that exhumation may be induced by magmatic activity (Hawkesworth et al., 1995; Hill et al., 1995). Stress and strain geometries may be a response to the rise of magmatic rocks and heat advection, which causes instabilities in the lithosphere and triggers the formation of core complexes.

2. Geological setting

2.1. Eastern Desert

Neoproterozoic rocks of the Arabian-Nubian Shield are exposed in the Central Eastern Desert of Egypt as a result of flank uplift triggered by the Red Sea rift (Garfunkel, 1988; Omar et al., 1989). The rock assembly is commonly subdivided into two major tectonostratigraphic units: (i) the lower unit constitutes the structural basement which occurs within fault-bounded core complexes (e.g. Meatiq, Sibai) and is referred to as 'infrastructure' by Habib et al. (1985), El Gaby et al. (1990), (ii) the structurally overlying nappe assemblage includes ophiolites (Shackleton et al., 1980), related metavolcanic and metasedimentary rocks as well

as molasse-type sediments and occupies the largest part of the Neoproterozoic rocks exposed in the Central Eastern Desert. This unit is here summarised as Pan-African Nappe Complex (Fig. 1) and was referred to as 'suprastructure' by El Gaby et al. (1990).

A simplified lithostratigraphy (for details see El Gaby et al., 1990; Greiling et al., 1994) of the infrastructure (i) from bottom to top includes: (1) Amphibolites, amphibolite migmatites and partly migmatic gneisses. They are abundant in the Hafafit area, occur as inclusions within the Um

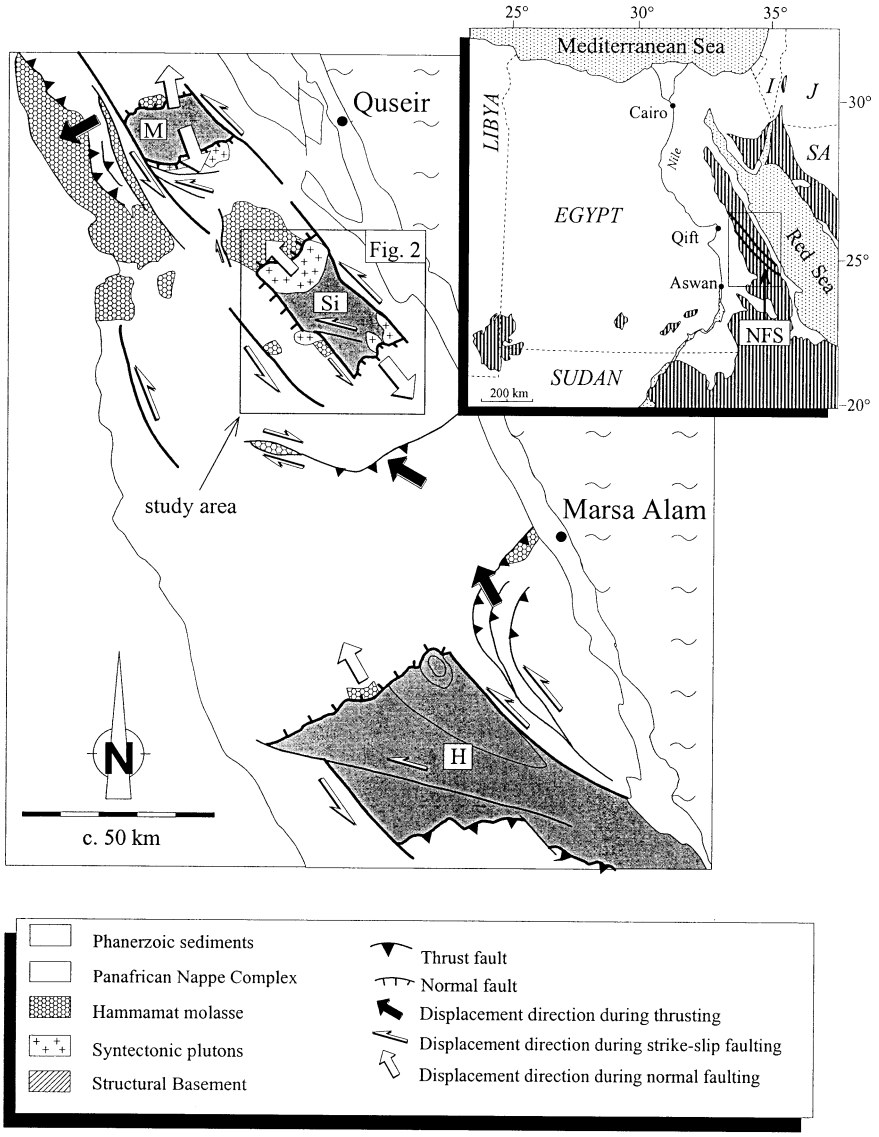

Fig. 1. Distribution of metamorphic and magmatic core complexes (M, Meatiq; Si, Sibai; H, Hafafit) and structural basement in the Pan-African Orogen in the Eastern Desert of Egypt (modified after Fritz et al., 1996). Slacking structures are indicated by black arrows. Structures related to extension and exhumation (white arrows) partitioned into strike slip displacements and low-angle normal shear zones along the Najd Fault System. Insert, Neoproterozoic outcrops of the Arabian-Nubian Shield (shaded) in the Eastern Desert of Egypt, Saudi Arabia (SA), Sudan and Libya. I, Israel; J, Jordan; NFS, Najd Fault System.

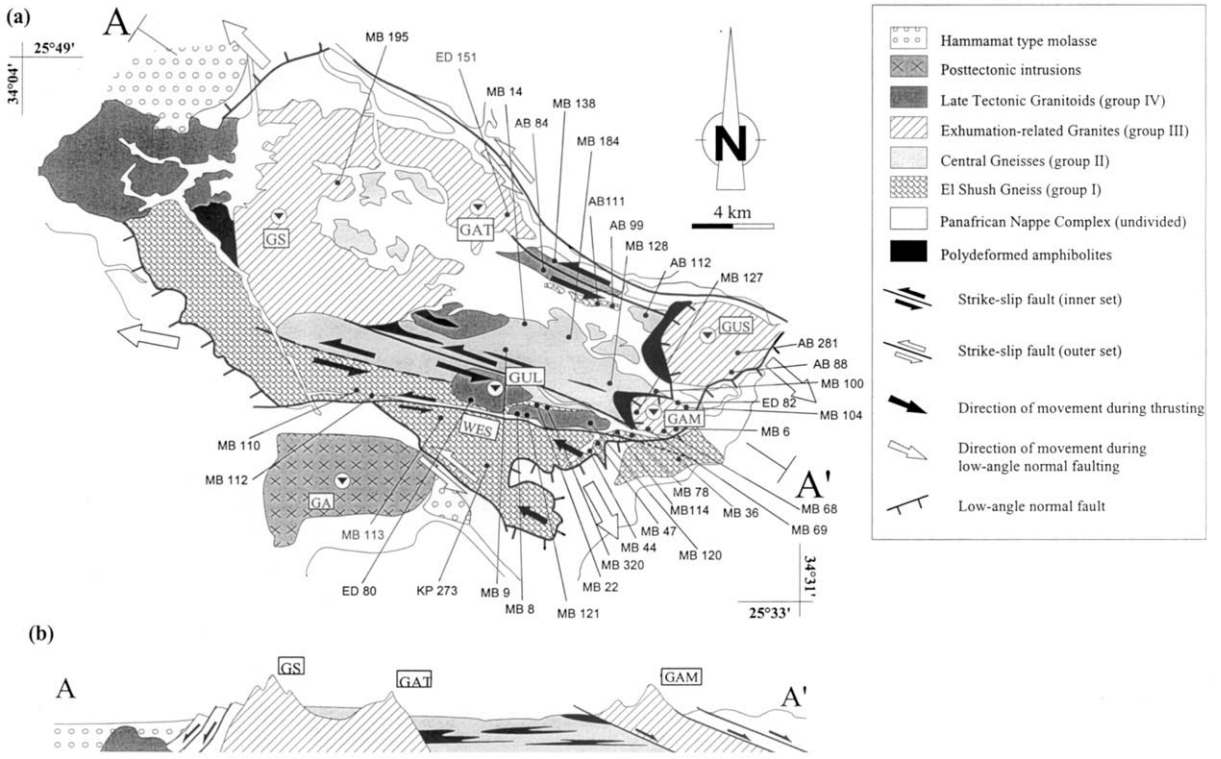

Fig. 2. (a) Schematic map of the Sibai core complex modified after Khudeir et al. (1995). Locations of samples (e.g. AB 186) for geochemical and geochronological investigations are shown. GS, Gebel Sibai; GAT, Gebel Abu Tiyur; GUL, Gebel Urn Luseifa; GUS, Gebel Um Shaddad; GAM, Gebel Abu Markhat; WES, Wadi El Shush; GA, Gebel Atawi. (b) Schematic profile from northwest to southeast outlining the different geometry of detachment shear zones in the northwest and southeast, respectively.

Ba'anib gneiss of the Meatiq Core Complex (Neumayr et al., 1998; Loizenbauer et al., 2001), but are reduced to small, elongated lenses in the Sibai Core Complex. (2) Tonalitic to granodioritic gneisses intruded the former suite (Rashwan, 1991; Kamal El Din, 1993; Neumayr et al., 1995). They were described as I-type calc-alkaline intrusive assemblage in the Hafafit area with protolith emplacement ages ranging from 677 to 700 Ma (Kröner et al., 1994). In the Sibai Core Complex, they are represented by the El Shush Gneiss unit of group (I) (Kamal El Din, 1993) (Fig. 2); in the Meatiq Core Complex equivalent rocks are rarely found (Loizenbauer et al., 2001). According to Kröner et al. (1994), granitoid members of this suite can be correlated with the so called 'Older Granites' of Egypt. (3) Highly-deformed metasedimentary sequences which are exposed in upper structural levels include aluminous metapelites, metapsammites and subordinate amphibolites (Neumayr et al., 1995). These overlie the Um Ba'anib gneiss in the Meatiq Core Complex (Loizenbauer et al., 2001) and are exposed as partly migmatised gneisses at Hafafit (Rashwan, 1991; El Ramly et al., 1993; Greiling et al., 1994). No representatives of this group are exposed at Sibai. (4) Late Neoproterozoic syntectonic granitoids intruded during orogen-parallel extension. They postdate thrusting of the Pan-African Nappe Complex, form most of the Sibai Core Complex and also occur at Meatiq and Hafafit. Part of them are referred to as 'Younger Granites' by Greenberg (1981).

The varied lithology of the Pan-African Nappe Complex (ii) is described from a cross section west of Quseir (Ries et al., 1983; Hassan and Hashad

1990; O'Connor, et al., 1994; Fritz et al., 1996) and includes from bottom to top: (1) An ophiolitic sequence of MORB or IAT affinity and volcano-sedimentary rocks (Shackleton et al., 1980; Al Shanti and Gass, 1983; Hassan and Hashad, 1990). The ages of the ophiolites range between 900 and 740 Ma (Ries et al., 1983; Kröner, 1985; Kröner et al., 1992, 1994; Loizenbauer et al., 2001). (2) Younger metavolcanics which consist of porphyritic, felsic and mafic rocks comparable to the Um Samiuki sequence date at approximately 710 Ma (Stern et al., 1991). (3) Subduction related plutonic and volcanic rocks of the Dokhan suite gave Rb/Sr isotopic ages of 655 Ma (Hashad et al., 1972) and 622 Ma (Stern and Hedge, 1985). (4) Molasse type sediments of the Hammamat series developed in the western portion of the Central Eastern Desert and in intramontane basins (Grothaus et al., 1979; Rice et al., 1993; Messner et al., 1996; Fritz and Messner, 2000). A late to post-Neoproterozoic age of thrusting in the Pan-African Nappe Complex is indicated by the incorporation of Hammamat rocks dating at approximately 590 Ma (Willis et al., 1988).

The intrusion of granites in the Central Eastern Desert peaked in two major phases of magmatic activity. During the first phase (ca. 800–700 Ma), the calc-alkaline Older Granites were formed (Kröner et al., 1990; Stern and Manton, 1987). In a second phase (ca. 650–550 Ma) the alkaline Younger Granites were generated and partly deformed by late Neoproterozoic tectonic activity (Greenberg, 1981). Beyth et al. (1994) concluded that the transition from calc-alkaline to alkaline magmatism occurred around 610 Ma in the northernmost part of the Arabian-Nubian Shield. Post-tectonic granitoids with circular shape penetrate both the Pan-African Nappe Complex and core complexes and cluster around 580 Ma (Sturchio et al., 1983).

Metamorphic core complexes in the Eastern Desert were first described by Sturchio et al. (1983). They are bounded by northwest–southeast striking, sinistral strike-slip shear zones and interlinking northwest or southeast dipping low-angle normal shear zones (Wallbrecher et al., 1993a,b; Greiling et al., 1993, 1994; Unzog and Kurz, 2000) (see Fig. 1). The sinistral strike-slip shear zones are interpreted to be the African counterpart of the Najd Fault System of the Arabian Peninsula (Stern, 1985). Core complexes are aligned subparallel with the strike of these strike-slip shear zones throughout the Proterozoic basement of the Central Eastern Desert. This situation is interpreted to represent a sinistral wrench corridor which is related to escape tectonism subsequent to oblique island arc accretion in the Neoproterozoic (Burke and Sengör, 1986; Stern, 1994; Fritz et al., 1996; Blasband et al., 2000; Fowler and Osman, 2001).

2.2. Geology of the Sibai area

The Sibai crystalline swell has first been recorded by Hume (1934) and interpretations of its geotectonic setting have been controversial ever since. Based on structural arguments the gneisses at Sibai have been regarded as pre-Neoproterozoic continental crust by El Gaby et al. (1984) and Khudeir et al. (1992, 1995). Alternatively, an evolution during island are accretion in the Neoproterozoic has been proposed for the Sibai gneisses (Kamal El Din, 1993; Greiling et al., 1994).

The fault systems enclosing the Sibai Core Complex (Fig. 2) consist of two parallel sinistral strike-slip shear zones (external set of strike-slip shear zones) in the northeast and southwest which are interlinked by normal shear zones in the northwest and southeast, respectively. This is similar to the Meatiq Core Complex approximately 50 km northwest of Sibai. (Fig. 1) and was interpreted to reflect northwest–southeast directed orogen-parallel extension (Fritz et al., 1996). A second set of sinistral, northwest trending strike-slip shear zones (internal set of strike-slip shear zones) developed within the structural basement of the Sibai (Fig. 2). Stacking structures such as duplexes of El Shush Gneiss and rocks of the Pan-African Nappe Complex are found south of Wadi El Shush (Fig. 2). They are related to northwest-vergent nappe transport predating transpression and orogen-parallel extension along the wrench corridor.

In this study, the Sibai Core Complex is divided into four groups of variably deformed granitoids based on petrography, geochemical composition, structural setting and age (Table 1). Metamorphic mineral reactions are restricted to those which occurred during cooling of the granitoids and the country rock. It shall be stressed here that no evidence for polymetamorphism, as demonstrated in other parts of the Central Eastern Desert (Neumayr et al., 1998), is evident from the Sibai granitoids.

2.2.1. Group (I): El Shush Gneiss

This group is most prominent in the southwestern part of the Sibai Core Complex, but also forms a narrow strip along its northeastern margin. The medium-grained rock shows an originally magmatic, granular, porphyritic fabric, locally with cataclastic overprint. Essential mineral assemblages are quartz, plagioclase, K-feldspar, biotile and actinolite with accessory apatite, zircon and sphene. Secondary formed minerals include sericite, epidote, zoisite, chlorite and muscovite. Epidote and zoisite occur in altered plagioclase porphyroblasts, actinolite and chlorite grow in pressure shadows of K-feldspar and plagioclase porphyroclasts, indicating deformation under metamorphic conditions that did not exceed greenschist facies. Retrograde minerals are abundant within zones of tectonic movement and enhanced fluid flow in the external areas of the dome. The weakly deformed tonalitic rocks are characterised by both magmatic and tectonic intercalation of amphibolites. Brittle–ductile to brittle overprint is common in the southwestern area, especially along the El Shush strike-slip fault and southeast dipping low-angle normal shear zones (Fig. 2). Duplex structures of metavolcanic rocks of the Pan-African Nappe Complex and the tonalitic gneisses are observed in the southeast, together with relic ductile, top-towards-northwest directed shear sense indicators within the gneisses. They represent the only stacking structures in the rocks of the Sibai Core Complex.

2.2.2. Group (II): Central Gneisses

Various types of granitoids forming the central part of the core complex are included within this

Table 1
Grouping of the granitoids in the Sibai core complex

Group	Sample number	Pb/Pb age (Ma)	Geochemical characteristic	Structural features
Group (I) El Shush Gneiss	MB 36, 44, 47, 110, 112, 113		VAG	Stacking structures
	MB 22, 78, 114, AB 99, 111			
	KP 273	694 ± 27 (mean)		
	MB 320	679 ± 7, 678 ± 8		
Group (II) Central Gneisses	MB 9, 14, 100, 128, AB 112	659 ± 14	WPG	Foliated parallel to stike-slip shear zones
	MB 184			
Group (III) Exhumation-related granites	MB 6, 68, 69, 104, 127, AB 88		WPG	Foliated parallel to low-angle normal shear zones
	ED 82	658 ± 16 (rim) 727 ± 16 (core)		
	AB 281	645 ± 5 (mean)		
	ED 151	653 ± 15		
	MB 195	654 ± 34, 657 ± 24		
Group (IV) Late tectonic granitoids	MB 8, 120, 121, 136, 137, 138		Variable	Margins follow older structures
	AB 84, ED 80			

VAG, volcanic arc granite; WPG, within-piate granite. Samples used for geochronological investigations are written in italic.

group. They are foliated parallel with the northwest–southeast trending strike-slip shear zones and show increasing deformation intensity from central to marginal portions (i.e. strain increases towards the internal set of Sibai strike-slip shear zones) (Fig. 2). They host a number of amphibolite xenoliths elongated along the general strike of the granitoids. Essential minerals are quartz, plagioclasc, K-feldspar, biotite; accessory minerals are apatite, zircon, sphene and secondary minerals include chlorite and epidote. The Central Gneisses show a porphyrilic texture with a fine-grained matrix of quartz, biotite, chlorite, plagioclase ± muscovite and porphyroblasts of K-feldspar. A modal estimation reveals a granodioritic to granitic composition.

2.2.3. Group (III): exhumation-related granites

These constitute the northwestern and southeastern portion of the core complex and truncate the group (II) gneisses either tectonically (in the southeast) or magmatically (in the northwest). The composite pluton of Gebel Sibai (GS) and Gebel Abu Tiyur (GAT) in the northwest of the Sibai (Fig. 2) is undeformed, of subcircular shape and with intrusive contact to deformed host rocks. The Gebel Abu Markhat (GUM) and Gebel Um Shaddad (GUS) gneisses in the southeast (Fig. 2) are internally deformed and exhibit distinct ultramylonites along their margins. Kinematic indicators display low-angle normal shear zone geometry (Bregar et al., 1996). Structures within GUM and GUS cut earlier formed deformation fabrics within the Central Gneisses (group II). The rocks of group III granitoids show a porphyritic fabric with a fine-grained matrix containing quartz, cataclastic feldspar and biotite. The porphyroblasts of plagioclase, K-feldspar and locally hornblende are up to 20 mm in length. Mineral assemblages include quartz, plagioclase, K-feldspar, hornblende, biotite; accessory minerals are zircon, apatite, sphene and epidote. Secondary minerals are sericite and chlorite. Elongated quartz grains, indicating low-temperature plasticity deformation mechanisms, are bent around rigid feldspar clasts. Feldspar is cataclastically deformed. Hornblende shows a zonation from green–brown cores to blue–green rims.

2.2.4. Group (IV) late tectonic granitoids

This variable group of weakly to non-foliated, leucocratic granitoids intrude groups (I), (II) and (III). The general trend of these elongated, comparatively small units is subparallel to the general strike of the group (II) units or parallel to pre-existing faults. Generally, they show a porphyritic texture that suffered weak tectonic overprint. Essential minerals are quartz, plagioclase, K-feldspar, muscovite, biotite, fluorite; accessory minerals are garnet, apatite, zircon and epidote; secondary minerals include scricite and chlorite. From estimated modal mineral contents the rocks cover the field of alkali-granite. The presence of magmatic fluorite suggests that the group (IV) granitoids are highly differentiated and formed during a late- to postorogenic magmatic cycle.

The Pan-African Nappe Complex surrounding the structural basement at Sibai consists of metavolcanic and metasedimentary rocks that were interpreted to have developed in an island are setting (Kamal El Din, 1993; Khudeir et al., 1995). The rock assemblage is dominated by epiclastic and volcanoclastic rocks in the northeast and east; by metagabbros and metavolcanic rocks in the southeast and south; and by serpentinites and metatuffs in the southwest. To the north the metavolcanic rocks are overlain by intramontane molasse sediments of the Wadi Kareim basin (Grothaus et al., 1979; Fritz and Messner, 2000), Basin sediments have been intruded by posttectonic group (IV) granitoids.

3. Kinematics and relative timing of magmatic and tectonic events

3.1. Kinematic development in the Eastern Desert

The core complexes in the Central Eastern Desert expose the magmatic or high-grade metamorphosed lower structural units of the Neoproterozoic basement. Structural cover units (Pan-African Nappe Complex) were detached from the northern and southern flanks of the domes during orogen-parallel extension. Major syntectonic subsidence adjacent to the core complexes is evident from deposition of intramontane

molasse-type Hammamat sediments (Kareim Basin: Fig. 2) (Fritz and Messner, 2000). The ubiquitous emplacement of synextensional granitoids and the intrusion of group (IV) granitoids into the molasse basins suggest enhanced temperatures during extension along the Najd Fault System. Stern (1985) interpreted the Najd Fault System as a late Precambrian rift-related transform system.

The Sibai magmatic core complex consists of basement domains tectonically separated from the Pan-African Nappe Complex. The geometry of detachment shear zones is similar to those of the metamorphic core complex at Gebel Meatiq. However, most of the basement of Sibai lacks prograde metamorphism. Stacking structures are abundant in the surrounding Pan-African Nappe Complex but are restricted to group (I) gneisses within the core complex. All other granitoid types exclusively exhibit structures related to NW–SE extension. Interrelations of the complex shear zone pattern and the succession of intrusions allow establishment of time relations between emplacement of various granitoids and progressively evolving structures. This provides insights into the dynamics of the formation of core complexes.

3.2. Deformation and granitoid intrusions

The rocks of group (I) are the only ones affected by northwest-directed thrusting. Structures include imbrications and duplex structures of El Shush Gneiss with rocks of the Pan-African Nappe Complex prior to the emplacement of granitoids of group (II), (III) and (IV) as well as relic, ductile, top-towards-northwest oriented shear sense indicators (Bregar, 1996). Apart from this domain of stacking in the southeast, the group (I) rocks occur along the most external southwestern and northeastern margins of the Sibai swell (Fig. 2). Their tectonic overprint is generally weak, brittle–ductile to brittle deformation occurs along faults (e.g. strike-slip fault in Wadi El Shush). The only strong overprint is known from the southeast, where group (I) rocks have been affected by southeast-directed normal faulting.

Group (II) rocks constitute the major part of the central Sibai Core Complex. They exhibit northwest–southeast trending, subvertical foliation and subhorizontal stretching lineation (Fig. 3). Deformation intensity, outlined by spacing of foliation planes and progressive grain size reduction, increases from internal portions symmetrically towards the northeastern and southwestern margins, respectively. These high strain zones represent the internal set of strike-slip zones in the Sibai.

The southeastern margin of the core complex is outlined by low-angle normal shear zones which truncate both, the group (II) gneisses and the internal set of strike-slip zones (Figs. 2 and 4). These normal shear zones define the structural margins along the footwall and the hangingwall of the synkinematically intruded group (III) granitoids represented by the Abu Markhat and Um Shaddad gneisses (Kamal El Din, 1993) and dip southeast at angles of 15–30°. Stretching lineation parallels the direction of dip (Fig. 3). Deformation intensity in the Abu Markhat gneiss increases dramatically from nearly-undeformed internal parts to ultramylonites in the footwall and hangingwall, respectively (Bregar et al., 1996; Unzog and Kurz, 2000). Deformation intensity and the shallow dips of the normal shear zones suggests that considerable northwest–southeast directed extension was accommodated by this deformation along the southern portions of the Sibai.

To the northwest of the Sibai, group (II) rocks and the internal pair of strike-slip zones are discordantly cut by the Gebel Sibai and Abu Tiyur intrusion of group (III), demonstrating that the

Fig. 3. Orientation data of foliation and stretching lineation (equal area plot, lower hemisphere, density contours in multiples of random). (a) Foliation and (b) stretching lineation from southeastern normal shear zones, (c) foliation and (d) stretching lineation from group II (e) foliation and (f) stretching lineation in southwestern strike-slip shear zone, (g) foliation and (h) stretching lineation in northeastern strike-slip shear zone. Foliation planes in (c) show two maxima, a steep one parallel to the strike-slip shear zones which dominates most of the central part of the core complex and a flat one which is due to overprint by the low-angle normal shear zones in the southeast.

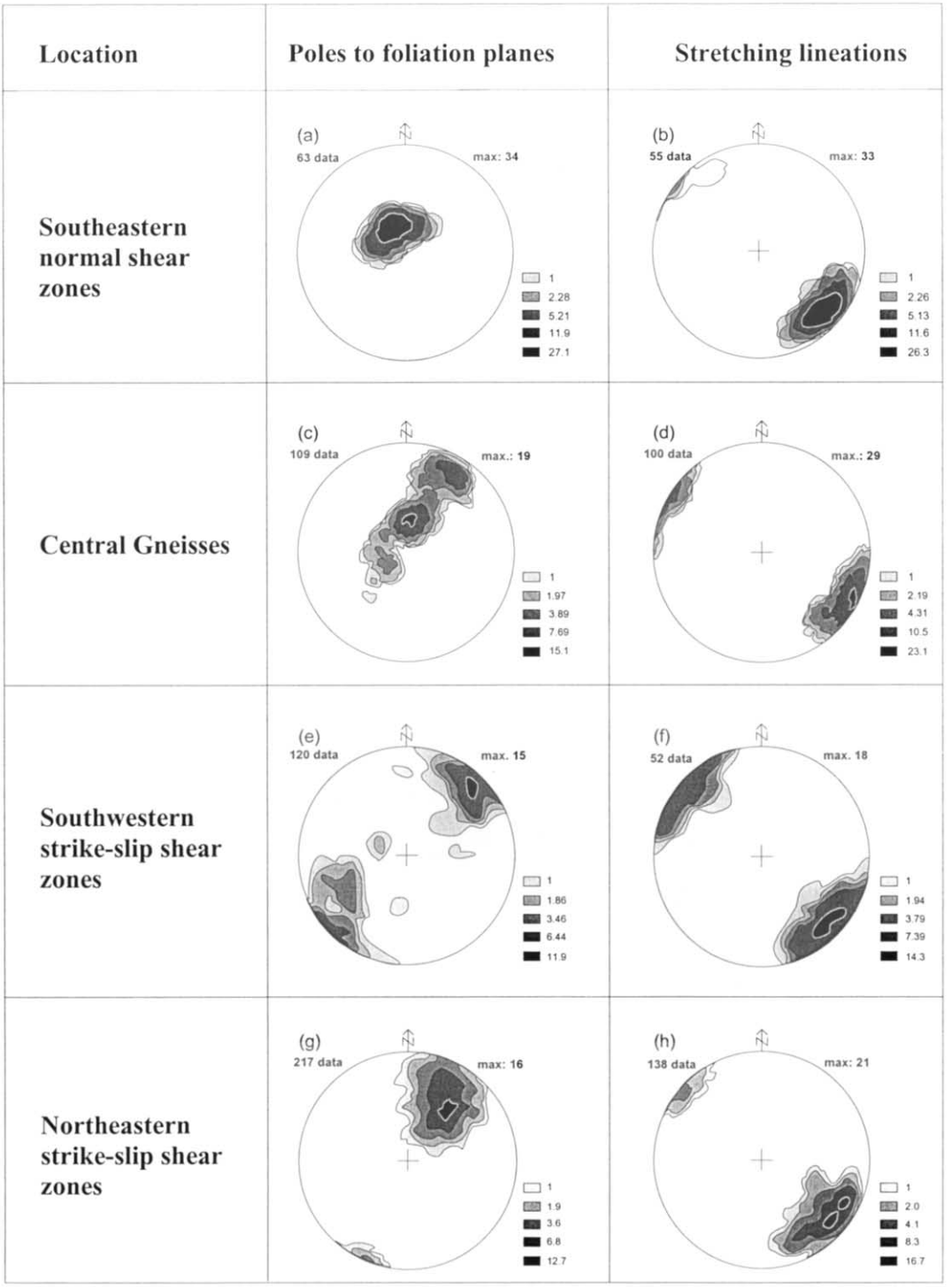
Location
Poles to foliation planes
Stretching lineations
Southeastern normal shear zones
(a)
63 data
max: 34
1
2.28
5.21
11.9
27.1
(b)
55 data
max: 33
1
2.26
5.13
11.6
26.3
Central Gneisses
(c)
109 data
max.: 19
1
1.97
3.89
7.69
15.1
(d)
100 data
max.: 29
1
2.19
4.31
10.5
23.1
Southwestern strike-slip shear zones
(e)
120 data
max. 15
1
1.86
3.46
6.44
11.9
(f)
52 data
max. 18
1
1.94
3.79
7.39
14.3
Northeastern strike-slip shear zones
(g)
217 data
max: 16
1
1.9
3.6
6.8
12.7
(h)
138 data
max: 21
1
2.0
4.1
8.3
16.7

Fig. 3.

intrusion of group (II) granitoids and the formation of the internal strike-slip shear zones predate the emplacement of the group (III) granites. Northwest of the latter, normal faults dipping to the northwest at angles of 45–50° formed within the Pan-African Nappe Complex and triggered sedimentation of the Wadi Kareim molasse basin. Provenance studies show that basal strata of the basin include pebbles of group (I) gneisses. Fritz and Messner (2000) reported that these basal conglomerates have subsequently been intruded by granitoids of group (IV). Both the southeastern and northwestern normal shear zones are associated with an external pair of sinistral strike-slip shear zones (Figs. 2–4) that curve smoothly around group (III) granitoids and thus post-date emplacement of these rocks. The external shear zones mark the boundary to the Pan-African Nappe Complex in the northeast and southwest. They developed under low-grade metamorphic conditions and deformation continued to brittle–ductile conditions.

The group (IV) granitoids represent highly differentiated, heterogeneous microgranitic to porphyritic rocks that occur as small elongated bodies within older granites. Their emplacement is largely controlled by and parallels pre-existing structures (Fig. 2). They are generally undeformed and represent the youngest magmatic event in the Sibai basement.

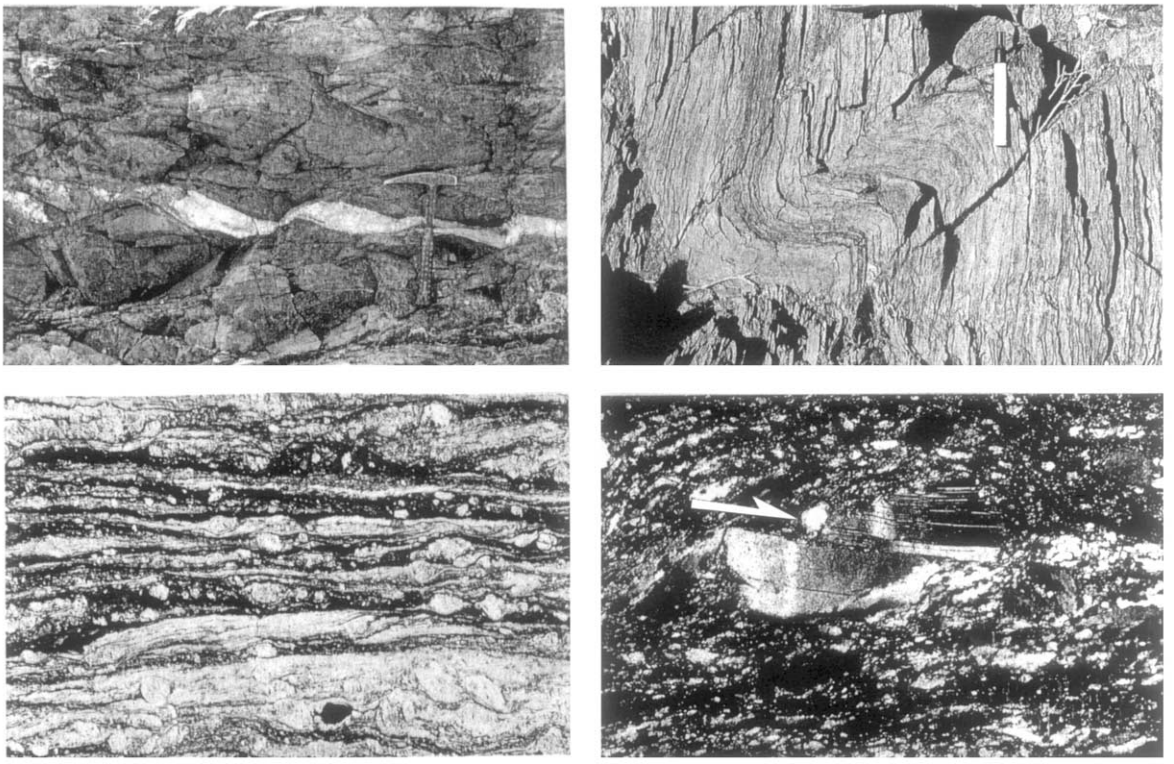

Fig. 4. Upper row, map views of sinistral shear fabrics from the northwest trending, steeply dipping external shear zone along the northeastern Sibai margin. See field equipment for scale. Upper left, sinistral shear from asymmetry of sheared and back-rotated vein (upper left corner is NW). Upper right, sinistral shear from vortex structure including vertical foliation and vertical fold axes. Upper side of photo is NW. Lower row, thin sections from the southeast dipping shear zones along the southern Sibai margin (upper right of pictures is southeast). Lower left, top to the southeast shear within mylonites from the Gebel Um Shaddad gneiss. Fabric asymmetries include S-C structures and ecc shear bands (long side of photo is 7.5 mm). Lower right, top to the southeast shear from synthetically sheared feldspar within quartz matrix (long side of photo is 3.8 mm).

3.3. Summary of kinematic and magmatic development

Based on interrelations between successively evolving structures and magmatism, a clear relative sequence of events may be established. Group (I) gneisses are interpreted to reflect the oldest magmatic event, since they record the only nappe stacking structures preserved in the Sibai Core Complex. All other units exhibit structures related to extension and are interpreted to have evolved progressively in the course of exhumation of the Sibai Core Complex. The inner set of strike-slip shear zones formed during an early stage of orogen-parallel extension. Deformation within these shear zones goes along with the emplacement and subsequent cooling of the group (II) gneisses which simultaneously suffered penetrative deformation. The arrangement of the external strike-slip and normal shear zones corresponds to a pull-apart like geometry suggesting that the dome formed in a shear-extensional setting of crustal scale. Topographic relief formed during activity of normal shear zones as documented by syntectonic sedimentary basins. Continuous northwest–southeast directed extension goes along with the intrusion of group (III) granites in the northwest and southeast, respectively. They crosscut the internal set of strike-slip shear zones and are deformed by both the low-angle normal shear zones and the successively evolving set of external strike-slip shear zones. Youngest strike-slip deformation is localised at the periphery of the dome where subvertical shear zones curve around the granitoid bodies of group (III).

In the southeast, a large offset along the low-angle normal shear zones accounts for the tectonic exhumation of the core complex. In the northeast, sedimentation within the Kareim molasse basin reflects the tectonic and magmatic history: clasts of the older group (I) gneisses were deposited within basal strata, while younger group (IV) granites intruded the Hammamat rocks and produced contact metamorphism. Subsidence of the basin was accompanied by high-angle normal faulting (Fig. 2b).

4. Pb/Pb ages of granitoids

4.1. Analytical techniques

Single zircon evaporation dating followed a modified procedure originally described by Kober (1987). Full details of the technique are reported in Klötzli (1997). Prior to analysis, the zircons were washed in warm high-purity HNO_3 for half an hour, rinsed with sub-boiled water and dried. A double Re filament arrangement in a FINNIGAN MAT 262 mass spectrometer equipped with an ion counter and a quotient pyrometer was used. Single zircon crystals were encased in the evaporation filament. The zircons were heated stepwise to 1200–1300 °C in order to strip off common Pb and radiogenic Pb components with low activation energies. As soon as no 'low-temperature' Pb was present, the zircon temperature was raised by 20 °C steps and evaporated Pb was deposited for 45 min on the cold ionisation filament and subsequently analysed for isotopic composition. After Pb analysis, the ionisation filament current was raised to 4.5 A for several seconds stripping off all remaining material deposited during the evaporation step. Then the next evaporation analysis cycle started. Evaporation temperatures were raised by approximately 20 °C from step to step until Pb evaporation from the zircon was complete. Depending on crystal quality, size, age, U and Pb content of the zircons one to six evaporation analysis cycles could be made.

Ion beam intensities were measured in blocks of ten scans with 4 s integration time and 2 s delay time each using dynamic or static acquisition procedures depending on ion beam intensity. The background was measured on half-masses every five blocks. The background correction was made on-line during data acquisition. Data acquisition comprised two to 20 blocks. $^{207}Pb/^{206}Pb$ and $^{208}Pb/^{206}Pb$ ratios were corrected using correction factors derived from NBS SRM 982 standard measurements. Lead fractionation is typically in the range of 0.11% per mass unit ($\pm$ 30%).

Only high temperature steps (>1300 °C) with $^{204}Pb/^{206}Pb < 0.00005$ were used for age calculations. Therefore, no common Pb correction had

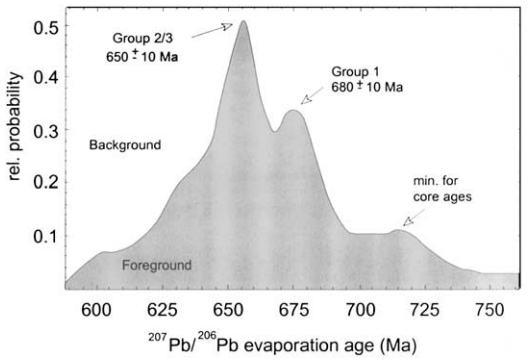

Fig. 5. Probability density distribution for the various mean age values compiled from 33 single measurements. Peaks outline the major magmatic events in the Sibai core complex.

to be applied. Age calculation and error statistics were made using the ISOPLOT software package of Ludwig (1992). Reported ages and errors are propagated weighted mean values calculated from at least 20 measured $^{207}Pb/^{206}Pb$ ratios. All errors reported are two standard errors (S.E.) of the mean (ca. 95% confidence limit).

4.2. Results

Analytical results are given in Table 2, for location of samples see Fig. 2. Mean values are summarised in Fig. 5. All zircons exhibit large variations in $^{208}Pb/^{206}Pb$, typically with low ratios in the lower temperature steps and higher ratios for the high temperature steps and systematic variations within the individual temperature steps (Fig. 6).

Group (I): from sample MB 320, two zircons give $\pm$ identical ages of 678 ± 8 and 679 ± 7 Ma, respectively. Results from sample KP 273 arc somewhat inconsistent. Zircon KP 273/A provided only one temperature step with a poorly constrained age of 705 ± 100 Ma. KP 273/B gives a mean age of 643 ± 436 Ma for three temperature steps. The second temperature step of this zircon at 1460 °C results in an age of 646 ± 52 Ma. Step 3 at 1500 °C gives an age of 698 ± 23 Ma. The weighted mean for KP 273/B is 681 ± 21 Ma which is close to sample MB 320.

Group (II): sample MB 184 provides an age of 659 ± 14 Ma.

Group (III): two zircons from sample MB 195 exhibit ages of 654 ± 34 and 657 ± 24 Ma, respectively. The zircon of sample EDI 51 gives a mean age of 653 ± 15 Ma over four temperature steps. Three zircons of sample AB 281 give ages of 650 ± 9, 636 ± 57 and 646 ± 17 Ma, resulting in a mean age of 645 ± 5 Ma. Sample ED 82 exhibits a low temperature evaporation age of 658 ± 16 Ma and a high temperature evaporation age of 727 ± 16 Ma.

4.3. Interpretation

Except for the core age of sample ED 82 (727 ± 16 Ma) all ages are interpreted as dating zircon growth during a magmatic event. The typical large variations in $^{208}Pb/^{206}Pb$ at constant $^{207}Pb/^{206}Pb$ together with the locally observed inverse deposits are interpreted to reflect changes in the Th/U ratio due to magmatic zonation in the zircons (Klötzli and Parrish, 1996; Klötzli, 1999) (Fig. 6). Thus the ages of group (II) and group (III) rocks, identical within error between 643 and 659 Ma (samples ED 151, ED 82, AB 281, MB 195, and MB 184), are interpreted to represent one progressive magmatic event in the Sibai Core Complex around 650 ± 10 Ma which we relate to orogen-parallel extension. The mean age of sample MB 320 of 679 Ma as well as the age of one zircon in sample KP 273 (705 Ma) possibly point to an older magmatic event which is interpreted to

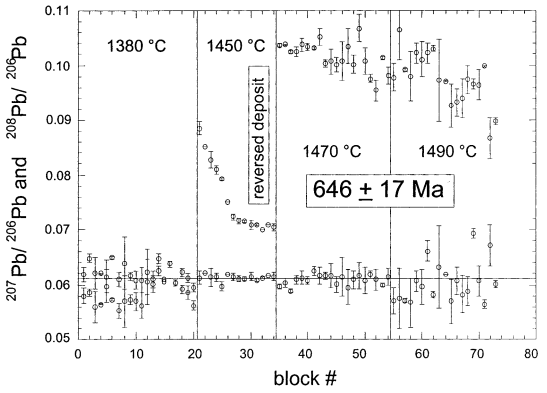

Fig. 6. Example of evaporation spectrum showing typical large variations of $^{208}Pb/^{206}Pb$ at constant $^{207}Pb/^{206}Pb$ for one zircon of sample AB 281 (four temperature steps).

Table 2
Geochronological results of the Sibai granitoids

Sample	Block	Evaporation temperature (°C)[a]	$^{207/206}Pb$[b]	2σ[c]	2σ (%)[c]	$^{207/206}Pb$ age (Ma)[d]	2σ (Ma)[b]	2σ (%)[b]	$^{208/206}Pb$[b]
KP 273/A/1	20	1450	0.06290	0.00300	4.8	705	100	14.2	0.0614
KP 273/B/1	6	1420	0.06100	0.01200	19.7	639	430	67.3	0.0410
KP 273/B/2	12	1460	0.06120	0.00150	2.5	646	52	8.1	0.0470
KP 273/B/3	20	1500	0.06271	0.00067	1.1	698	23	3.3	0.0498
KP 273 mean			0.06258	0.00078	1.2	694	27	3.8	
MB 320/A/1	20	1430	0.06199	0.00038	0.6	674	13	1.9	0.0207
MB 320/A/2	20	1500	0.06216	0.00037	0.6	680	13	1.9	0.0444
MB 320/B/1	20	1450	0.06208	0.00040	0.6	677	14	2.1	0.0444
MB 320 mean			0.06213	0.00020	0.3	679	7	1.0	
MB 184/A/1	6	1400	0.06185	0.00078	1.3	669	28	4.2	0.0848
MB 184/A/2	20	1400	0.06142	0.00039	0.6	654	14	2.1	0.0852
MB 184 mean			0.06156	0.00039	0.6	659	14	2.1	
ED 82/A/1	9	1365	0.05680	0.00490	8.6	484	190	39.3	0.0356
ED 82/A/2	9	1355	0.06200	0.00140	2.3	674	49	7.3	0.0649
ED 82/A/3	15	1385	0.06149	0.00031	0.5	656	11	1.7	0.0640
ED 82/A/4	5	1406	0.06447	0.00002	0.0	757	1	0.1	0.0949
ED 82/A/5	8	1427	0.06326	0.00054	0.9	717	18	2.5	0.1073
ED 82/A/6	3	1446	0.06338	0.00085	1.3	721	28	3.9	0.1130
ED 82 mean (rim)			0.06154	0.00047	0.8	658	16	2.5	
ED 82 mean (core)			0.06355	0.00049	0.8	727	16	2.2	
AB 281/A/1	10	1400	0.06144	0.00053	0.9	655	19	2.9	0.0773
AB 281/A/2	14	1460	0.06116	0.00048	0.8	645	17	2.6	0.0942
AB 281/A/3	8	1480	0.06140	0.00200	3.3	653	71	10.9	0.1060
AB 281/A/4	14	1545	0.05940	0.00320	5.4	582	120	20.6	0.1244
AB 281/B/1	10	1450	0.05590	0.00720	10.9	803	230	28.6	0.0932
AB 281/B/2	12	1470	0.05980	0.00240	4.0	596	84	14.1	0.0967
AB 281/B/3	11	1490	0.06100	0.00260	4.3	639	92	14.4	0.1030
AB 281/C/1	20	1380	0.06205	0.00077	1.2	676	26	3.9	0.0578
AB 281/C/2	14	1450	0.06147	0.00024	0.4	656	8	1.3	0.0757
AB 281/C/3	20	1470	0.06075	0.00037	0.5	630	13	2.1	0.1020
AB 281/C/4	20	1490	0.05380	0.00140	2.3	596	52	8.7	0.0987
AB 281 mean			0.06116	0.00013	0.2	645	5	0.7	
ED 151/A/1	7	1364	0.05110	0.00073	1.2	643	26	4.0	0.0920
ED 151/A/2	10	1404	0.61390	0.00085	1.4	653	30	4.6	0.1302
ED 151/A/3	11	1424	0.06156	0.00078	1.3	659	28	4.2	0.1467
ED 151/A/4	5	1444	0.06050	0.00170	2.8	622	63	10.1	0.1373
ED 151 mean			0.06139	0.00043	0.7	653	15	2.3	
MB 195/A/1	20	1490	0.06140	0.00210	3.4	653	75	11.5	0.1247
MB 195/A/2	20	1490	0.06145	0.00089	1.4	655	30	4.6	0.1262
MB 195/B/1	20	1382	0.06170	0.00180	2.9	664	64	9.6	0.1388
MB 195			0.06152	0.00069	1.1	657	24	3.7	

[a] Error on evaporation temperature is estimated to be ±10 °C.
[b] Weighted mean from individual scan ratios.
[c] All errors reported are two S.E. of the mean.
[d] Mean ages derived from individual scan ratios and not from individual scan ages.

have occurred during island arc accretion. The core ages from sample ED 82 (727 ± 16 Ma) have to be interpreted as representing minimum ages for older zircon growth or recrystallisation.

Summarising the radiometric data for the Sibai Core Complex (Fig. 5) and bearing in mind that zircon evaporation data reflect minimum ages we conclude that (1) there is no pre-Neoproterozoic crust represented by the Sibai granitoids, (2) group (I) rocks, which exhibit stacking structures are distinctly the oldest rocks (680 ± 10 Ma), (3) Pb/Pb data do not resolve the relative ages of group (II) and III (650 ± 10 Ma) which is clearly proposed from the field investigations, therefore, a rather rapid evolution during the orogen-parallel extension has to be assumed.

5. Geochemistry

The samples were cleaned with water and the weathering crust removed with a thin saw blade. Cutting marks were removed by grinding. After cleaning in water and drying, the samples were crushed in a jaw crusher, which was cleaned in between individual samples by analytically pure quartz. The ground samples were then powdered in a tungsten–carbide mill. Major-, trace- and rare earth elements (REE) have been analysed at the XRAL commercial laboratory in Don Mills, Canada. Initial calibration was performed against international rock standards. Machine performance was monitored by periodically analysing known standards. Analytical data including detection limits are given in Table 3.

5.1. Results

Results of geochemical data are plotted in various discrimination diagrams (Fig. 7) as well as in ORG normalised spidergrams (Fig. 8). In general there is a trend from calc-alkaline rocks of group (I) towards a more evolved chemistry of group (II) and group (III) which show A-type affinity. Data for group (IV) exhibit significant scatter. A short description of the concentrations of elements relevant for the discrimination plots of Fig. 7 is given below.

5.1.1. Group (I) El Shush Gneiss

These granitoids are characterised by the lowest SiO_2 (64.80–73.00 wt.%) and K_2O (0.50–2.40 wt.%) concentrations of all analysed rocks, whereas Al_2O_3 (13.70–17.30 wt.%), MgO (0.60–1.95 wt.%) and CaO (2.40–5.85 wt.%) are highest. Also TiO_2 is higher than in most other samples (0.20–0.40 wt.%). This granitoid type typically shows high Sr (147–584 ppm) and Ba (156–516 ppm) contents, but low Zr (69–142 ppm) concentrations. Niobium is particularly low, around 10 ppm. Both light and heavy REE are also low.

5.1.2. Group (II) Central Gneisses

The Central Gneisses show intermediate SiO_2 concentrations (70.20–74.50 wt.%). All other major elements are also intermediate, (e.g. Al_2O_3, 13.30–15.00 wt.%; FeO, 1.25–2.40 wt.%; MgO, 0.32–0.40 wt.%; CaO, 1.08–2.13 wt.%; K_2O, 2.75–4.30wt.%). The Central Gneisses are typically poor in trace elements such as Nb (20–31 ppm), and intermediate in Y (32–61 ppm), Sr (129–222 ppm) and Ba (514–838 ppm). Zirconium is intermediate in most samples of this group and Rubidium is high with 50–134 ppm. The LREE and the HREE are marginally elevated compared with the other groups.

5.1.3. Group (III) exhumation-related granites

The group (III) samples arc typically low in TiO_2 (0.10–0.20 wt.%) and lowest in Al_2O_3 (10.30–12.30 wt.%). The rocks are particularly poor in MgO (0.04–0.20 wt.%) and CaO (0.20–0.70 wt.%). The SiO_2 content is very high (75.90–80.20 wt.%). Sodium (2.30–3.50 wt.%) is lower than in all other suites. This rock type belongs to the groups with highest K_2O concentrations, which range from 3.85 to 4.80 wt.%. Trace elements such as Sr (73–118 ppm) are generally low. Barium concentrations (597–1230 ppm) are highest compared with all other rock types. Zirconium (208–370 ppm), Nb (3l–46 ppm) and Y (52–95 ppm) are also high.

5.1.4. Group (IV) late tectonic granitoids

These samples are particularly rich in K_2O (3.40–4.40 wt.%) and variable in SiO_2 (68.90–77.10 wt.%) and $A1_2O_3$ (12.90–14.80 wt.%).

Table 3
Geochemical data of the Sibai granitoids

Unit	Group (I) El Shush Gneiss											Group (II) Central Gneisses						Group (III) Exhumation-related granites							Group (IV) Late tectonic granitoids							
Sample	MB 36	MB 44	MB 47	MB 110	MB 112	MB 113	MB 22	MB 78	MB 114	AB 99	AB 111	MB 9	MB 14	MB 100	MB 128	AB 112	AB 112	MB 6	MB 88	AB 33	MB 08	MB 127	MB 104	ED 82	MB 8	MB 120	MB 121	AB 34	ED 30	MB 136	MB 137	MB 138
SiO_2	71.70	68.50	68.00	69.10	69.50	68.60	64.80	57.80	57.20	88.00	73.00	70.20	70.50	74.10	74.30	74.50	74.50	80.20	75.80	75.90	78.40	77.40	78.10	77.90	75.90	76.40	74.30	76.30	58.90	77.10	75.40	70.50
TiO_2	0.23	0.27	0.26	0.37	0.22	0.30	0.35	0.33	0.36	0.35	0.21	0.38	0.31	0.21	0.22	0.15	0.15	0.11	0.14	0.17	0.15	0.16	0.14	0.14	0.03	0.04	0.13	0.01	0.62	0.03	0.04	0.03
Al_2O_3	15.00	16.00	13.70	16.10	16.70	15.80	17.30	16.80	16.10	15.70	14.50	14.20	15.00	13.50	13.30	13.70	13.70	10.30	12.20	12.30	10.60	11.40	11.30	11.10	13.40	13.10	13.60	13.70	14.80	12.00	13.30	13.10
Fe_2O_3	0.33	0.32	0.91	0.40	0.33	0.44	0.57	0.45	0.57	0.41	0.27	0.45	0.47	0.28	0.30	0.25	0.25	0.23	0.33	0.35	0.30	0.35	0.29	0.30	0.05	0.10	0.24	0.07	0.54	0.13	0.09	0.08
FeO	1.67	1.84	4.64	2.03	1.57	2.24	2.90	2.31	2.91	2.07	1.38	2.30	2.39	1.41	1.54	1.26	1.25	1.16	1.67	1.76	1.98	1.77	1.47	1.53	0.25	0.50	1.23	0.37	3.26	0.57	0.44	0.42
MnO	0.04	0.04	0.10	0.03	0.05	0.05	0.08	0.05	0.07	0.03	0.04	0.04	0.05	0.04	0.05	0.04	0.04	0.01	0.03	0.05	0.02	0.02	0.03	0.04	0.01	0.01	0.05	0.05	0.07	0.02	0.01	0.02
MgO	0.90	1.10	1.78	1.15	1.12	1.26	1.95	1.58	1.50	1.23	0.81	0.34	0.39	0.43	0.44	0.32	0.32	0.04	0.10	0.17	0.13	0.00	0.10	0.05	0.05	0.08	0.22	0.10	0.78	0.05	0.05	0.13
CuO	3.28	3.27	5.23	4.13	3.86	4.52	5.81	4.67	5.65	3.76	2.36	2.00	2.13	1.65	1.79	1.08	1.08	0.16	0.38	0.52	0.50	0.46	0.19	0.72	0.39	1.00	1.26	0.83	2.57	0.56	0.62	0.97
Na_2O	4.11	4.56	7.45	4.24	4.81	3.65	3.84	3.76	3.37	3.79	4.14	3.69	4.92	9.60	3.55	3.52	3.52	3.09	3.49	3.49	2.34	2.75	3.18	3.16	3.81	3.97	3.98	4.18	3.31	4.20	4.53	4.22
K_2O	0.98	1.52	0.53	1.07	1.22	1.33	1.22	1.14	0.70	2.11	2.42	3.51	2.75	3.70	3.41	4.34	4.34	3.35	4.25	4.63	4.53	4.81	4.50	4.41	4.39	3.82	4.04	3.83	3.70	3.99	4.18	3.37
P_2O_5	0.08	0.09	0.06	0.12	0.09	0.10	0.08	0.12	0.09	0.11	0.07	0.14	0.08	0.06	0.06	0.04	0.04	0.01	0.01	0.02	0.01	0.02	0.01	0.01	0.01	0.01	0.04	0.02	0.20	0.01	0.01	0.01
LOI	1.75	2.55	2.00	1.00	0.60	1.55	1.10	0.90	0.90	2.10	0.70	2.85	0.00	0.35	0.95	0.90	0.00	0.55	0.85	0.25	0.70	0.45	0.85	0.30	0.75	0.75	0.30	0.90	0.45	0.70	1.05	1.05
Total	100.05	99.95	99.67	99.76	100.18	99.84	99.79	99.91	99.72	99.68	99.70	100.10	99.89	99.83	99.92	100.09	100.09	99.61	100.02	99.60	99.80	99.88	99.95	99.66	100.07	99.78	99.99	100.13	99.70	100.36	99.71	99.90
Cr	15	6	11	13	6	10	26	12	18	9	6	5	5	18	5	7	7	10	2	6	18	13	6	7	5	11	18	10	3	33	13	8
Ni	6	2	3	3	2	1	14	3	4	5	2	1	1	1	4	2	2	3	2	7	1	1	3	2	14	1	1	17	8	1	1	12
Ca	6	6	16	8	7	10	12	9	10	9	5	5	190	3	220	270	270	310	160	67	2	3	240	220	2	2	3	2	88	2	2	1
Sc	5	5	25	2	5	6	12	6	15	4	4	6	4	5	5	4	4	1	3	4	2	7	3	3	0	1	3	3	7	1	1	2
V	34	31	129	42	27	50	78	41	73	39	23	18	11	18	17	18	18	3	2	2	2	4	2	2	2	2	5	2	28	2	2	2
Cu	9	9	20	8	13	19	18	2	6	17	7	3	4	4	3	3	3	3	2	3	5	10	3	3	1	2	3	4	7	4	3	2
Pb	2	2	2	2	2	2	2	2	2	2	3	2	2	8	3	2	2	2	3	2	2	4	3	3	8	12	2	8	2	11	8	7
Zn	43	55	51	59	68	61	62	61	58	58	48	45	96	66	60	52	52	27	68	133	41	28	62	86	11	30	62	21	84	47	42	15
Cd	1.00	1.00	1.00	1.00	1.00	1.00	1.00	1.00	1.00	1.00	1.00	1.00	1.00	1.00	1.00	1.00	1.00	1.00	1.00	1.00	1.00	1.00	1.00	1.00	1.00	1.00	1.00	1.00	1.00	1.00	1.00	1.00
W	1.00	1.00	1.00	1.00	1.00	1.00	1.00	1.00	1.00	1.00	1.00	1.00	1800.00	1.00	2100.00	2500.00	2600.00	2900.00	1600.00	890.00	1.00	1.00	2400.00	2000.00	1.00	1.00	1.00	1.00	870.00	1.00	1.00	1.00
Mo	2.00	2.00	2.00	2.00	2.00	2.00	2.00	2.00	2.00	2.00	2.00	2.00	2.00	2.00	2.00	4.00	4.00	12.00	3.00	2.00	2.00	2.00	17.00	8.00	2.00	2.00	2.00	2.00	2.00	2.00	2.00	2.00
As	1.00	1.00	1.00	1.00	1.00	1.00	1.00	1.00	1.00	1.00	1.00	1.00	1.00	1.00	1.00	1.00	1.00	1.00	1.00	1.00	1.00	1.00	1.00	1.00	1.00	1.00	1.00	1.00	1.00	1.00	1.00	1.00
Se	1.00	1.00	1.00	1.00	1.00	1.00	1.00	1.00	1.00	1.00	1.00	1.00	1.00	1.00	1.00	1.00	1.00	1.00	1.00	1.00	1.00	1.00	1.00	1.00	1.00	1.00	1.00	1.00	1.00	1.00	1.00	1.00
Sb	0.10	0.10	0.10	0.10	0.10	0.10	0.10	0.10	0.10	0.10	0.10	0.10	0.10	0.10	0.10	0.10	0.10	0.10	0.10	0.10	0.10	0.10	0.20	0.10	0.10	0.10	0.10	0.10	0.10	0.10	0.10	0.10
Ag	0.2	0.1	0.1	0.1	0.1	0.4	0.4	0.1	0.1	0.8	0.3	0.4	0.1	0.3	0.4	0.3	0.3	0.3	0.1	0.1	0.1	0.1	0.1	0.1	0.2	0.1	0.2	0.2	0.2	0.4	0.1	0.3
Au	2.0	2.0	3.0	2.0	2.0	2.0	3.0	2.0	2.0	2.0	2.0	5.0	2.0	3.0	2.0	2.0	2.0	2.0	2.0	6.0	2.0	2.0	2.0	2.0	5.0	2.0	2.0	10.0	2.0	10.0	7.0	5.0
Rb	24	34	75	28	28	37	39	39	30	57	64	71	50	102	117	134	134	50	81	91	72	83	96	55	131	154	141	133	89	127	130	65
Cr	0.80	0.80	0.80	0.50	0.50	0.80	0.90	0.90	0.90	1.00	1.30	1.10	0.50	0.90	2.70	2.10	2.10	1.00	1.00	1.20	0.70	0.90	0.70	0.80	0.70	2.90	1.40	1.60	1.80	0.80	1.10	0.60
Ba	430	320	209	309	315	516	309	357	158	484	303	712	838	514	549	574	574	597	761	995	1230	1130	964	918	198	95	322	23	914	51	68	175
Sr	387	454	147	553	584	465	466	513	518	384	257	204	222	129	149	147	147	73	78	85	118	98	87	88	135	76	109	58	268	48	40	90
Ta	0.50	0.50	0.50	0.50	0.50	0.50	0.50	0.50	0.50	0.50	0.60	0.50	3.90	2.00	8.50	8.50		8.70	5.20	3.50	2.60	1.50	5.50	6.70	0.50	2.10	3.10	1.30	2.80	3.20	3.60	0.50
Nb	10.0	10.0	10.0	10.0	10.0	10.0	10.0	10.0	10.0	10.0	11.0	20.0	31.0	23.0	30.0	29.0	29.0	41.0	45.0	41.0	46.0	31.0	33.0	33.0	10.0	18.0	41.0	13.0	25.0	39.0	46.0	10.0
Hf	2.70	2.20	2.00	2.70	2.70	3.00	1.80	3.20	2.60	3.60	3.90	9.90	0.20	6.20	0.20	0.20	0.20	0.20	0.20	0.20	9.70	10.00	0.20	0.20	4.50	3.60	5.70	3.60	0.20	10.00	8.10	1.60
Zr	97	87	69	108	90	96	76	109	93	142	110	329	403	166	185	151	151	208	300	311	313	352	370	364	95	70	146	38	383	165	104	34
Ti	1373	1595	1589	2230	1343	1775	2074	1954	2170	2098	1283	2254	1864	1258	1323	923	923	653	815	989	875	983	821	857	204	258	761	35	3135	204	240	162
Y	10	10	16	10	14	10	11	10	13	10	19	32	44	60	61	48	48	53	79	95	69	69	53	52	11	34	53	38	41	90	82	18
Th	2.40	2.60	1.10	3.70	3.20	1.40	2.70	1.50	0.50	3.00	6.60	13.00	5.20	8.00	11.00	0.80	9.00	7.70	10.00	7.90	13.00	11.00	7.40	8.50	4.90	14.00	13.00	5.70	12.00	7.70	10.00	5.50
U	0.60	0.50	0.50	0.50	0.80	0.70	0.50	0.40	0.60	0.60	1.30	2.20	1.50	2.50	5.20	3.40	3.40	2.40	3.50	2.00	4.10	2.60	1.80	1.40	4.00	4.80	6.30	1.40	2.90	4.00	3.90	2.40
La	13.50	15.00	3.90	27.80	10.50	7.90	10.50	7.30	3.70	19.20	17.80	64.70	50.10	29.10	33.40	26.10	26.10	66.60	85.40	102.00	99.40	133.00	111.00	105.00	2.50	6.80	34.00	6.90	68.70	3.60	4.70	7.50
Ce	24.00	27.00	10.00	48.00	34.00	16.00	22.00	13.00	8.00	34.00	33.00	120.00	96.00	58.00	69.00	55.00	55.00	132.00	173.00	161.00	189.00	245.00	208.00	205.00	5.00	20.00	68.00	16.00	127.00	14.00	17.00	16.00
Nd	10.00	10.00	6.00	19.00	12.00	8.00	10.00	6.00	5.00	11.00	13.00	51.00	48.00	27.00	32.00	20.00	28.00	58.00	76.00	102.00	82.00	105.00	91.00	85.00	3.00	11.00	33.00	10.00	55.00	11.00	14.00	9.00
Sm	1.76	1.91	1.59	2.87	1.98	1.68	2.05	0.90	1.85	1.58	2.88	9.48	8.53	5.01	7.00	5.93	5.93	10.90	15.00	22.50	16.60	18.10	16.40	14.80	0.64	4.21	7.40	2.91	10.00	5.29	6.44	2.01
Eu	0.66	0.45	0.46	0.83	0.66	0.48	0.73	0.63	0.69	0.92	1.05	1.98	2.49	0.91	0.94	1.40	1.40	1.92	2.06	2.55	2.53	3.07	2.85	2.90	0.95	0.36	1.25	0.15	1.73	0.15	0.32	0.57
Tb	0.20	0.30	0.20	0.30	0.30	0.20	0.20	0.10	0.20	0.10	0.40	0.80	0.80	1.20	1.10	0.80	0.80	0.40	1.70	3.00	2.20	2.30	1.90	1.40	0.10	0.90	1.30	0.60	1.00	1.80	2.10	0.30
Yb	0.43	0.57	2.14	0.30	0.42	0.78	1.04	0.36	1.03	0.24	1.14	2.47	3.90	5.94	5.67	4.13	4.13	5.80	7.17	7.13	8.79	5.93	5.14	4.27	0.72	3.23	5.47	3.09	3.36	68.20	7.95	1.64
Lu	0.06	0.08	0.35	0.04	0.08	0.12	0.17	0.06	0.17	0.04	0.18	0.37	0.03	0.93	0.92	0.66	0.66	0.83	1.10	1.02	0.00	0.81	0.72	0.63	0.16	0.47	0.85	0.44	0.52	1.25	1.19	0.27
Br	2.40	2.10	2.30	1.30	2.80	2.20	2.10	2.20	1.30	2.60	1.60	1.40	0.50	2.30	3.90	0.50	0.60	0.50	0.50	2.00	1.40	2.40	0.50	0.50	1.80	1.50	2.80	2.30	2.40	2.80	2.70	1.70
B	10.00	10.00	10.00	10.00	10.00	10.00	10.00	10.00	10.00	10.00	10.00	10.00	10.00	10.00	10.00	10.00	10.00	10.00	10.00	10.00	10.00	10.00	10.00	10.00	10.00	10.00	10.00	10.00	10.00	10.00	10.00	10.00
Be	1.00	1.00	1.00	1.00.	1.00	1.00	1.00	1.00	1.00	1.00	2.00	2.00	3.00	4.00	4.00	4.00	4.00	1.00	4.00	3.00	2.00	2.00	2.00	2.00	3.00	5.00	5.00	2.00	3.00	4.00	6.00	1.00

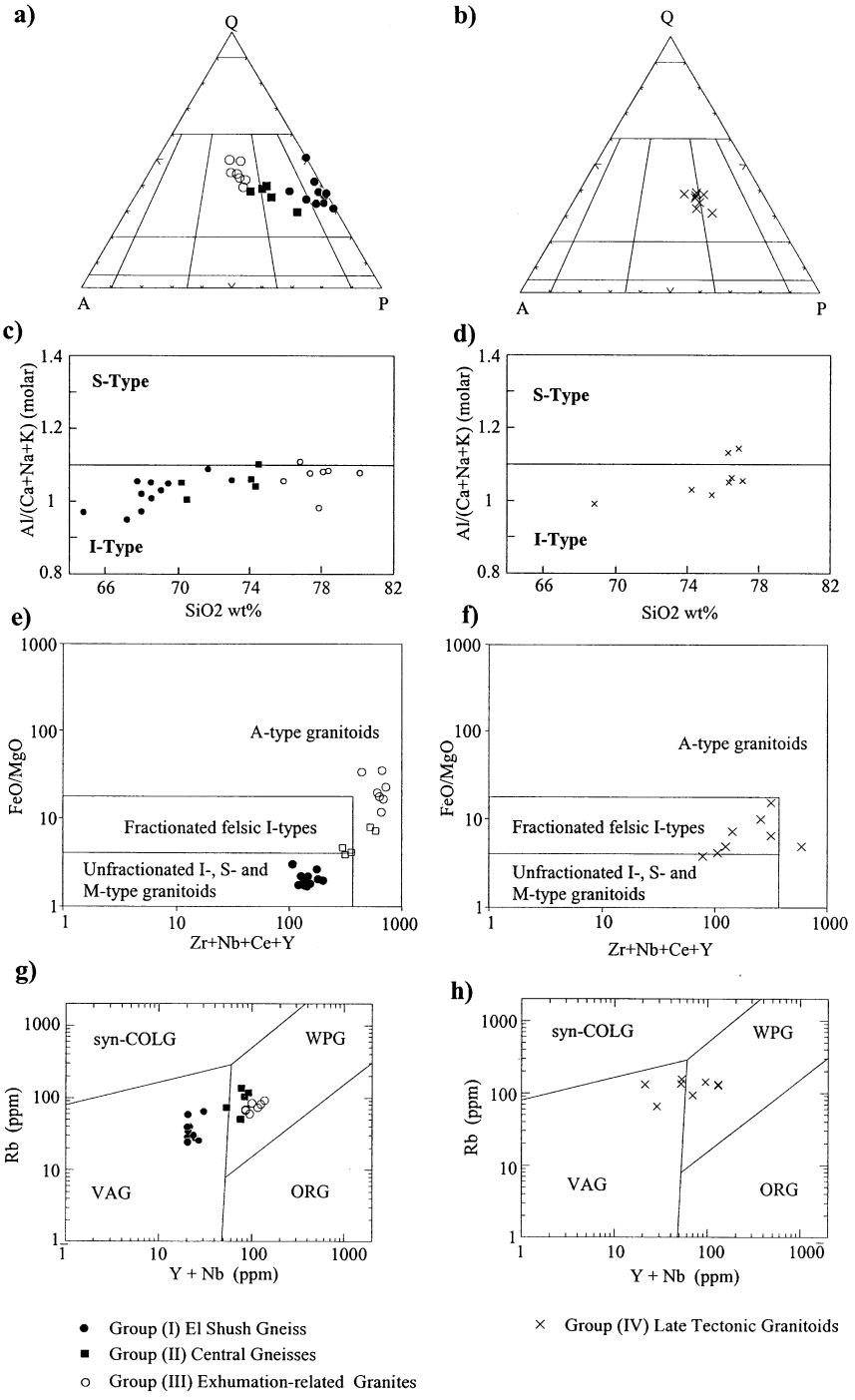
a)
Q
A
P
b)
Q
A
P
c)
Al/(Ca+Na+K) (molar)
S-Type
I-Type
SiO2 wt%
d)
Al/(Ca+Na+K) (molar)
S-Type
I-Type
SiO2 wt%
e)
FeO/MgO
A-type granitoids
Fractionated felsic I-types
Unfractionated I-, S- and M-type granitoids
Zr+Nb+Ce+Y
f)
FeO/MgO
A-type granitoids
Fractionated felsic I-types
Unfractionated I-, S- and M-type granitoids
Zr+Nb+Ce+Y
g)
Rb (ppm)
syn-COLG
WPG
VAG
ORG
Y + Nb (ppm)
h)
Rb (ppm)
syn-COLG
WPG
VAG
ORG
Y + Nb (ppm)
Group (I) El Shush Gneiss
Group (II) Central Gneisses
Group (III) Exhumation-related Granites
Group (IV) Late Tectonic Granitoids

Fig. 7.

Sodium (3.80–4.50 wt.%) approximates the concentrations in other granitoids except group (III). The other major elements are low (FeO, 0.30–3.30 wt.%) to extremely low (TiO_2, 0.01–0.50 wt.%; MgO, 0.01–0.80 wt.%; CaO, 0.40–2.60 wt.%). Trace elements are generally very low (Sr, 40–258 ppm; Zr, 34–383 ppm), although some elements show a considerable spread in their concentrations (Y, 11–90 ppm; Nb, 10–46 ppm). Barium is rather low (23–322 ppm) in most samples but with some reaching 914 ppm.

5.2. Interpretation

All samples plot within the granite, adamellite, granodiorite and tonalite fields of Debon and Le Fort (1983). The major bodies show a clear trend from group (I) gneisses in the tonalite field to group (III) in the granite field as displayed in the QAP plot (Fig. 7a). The group (IV) granites are variable in chemistry and cover the fields of granites to granodiorites in the mesonormative QAP plot (Fig. 7b).

From field relations and geochemistry all granitoids appear to be magmatic rocks. All granitoids are metaluminous except for some group (III) and (IV) gneisses, which are weakly peraluminous (Shand, 1927). The El Shush Gneiss is characterised by the lowest A/(2CNK) ratios (Shand, 1927), whereas most other samples cluster close to the metaluminous/peraluminous line. On the other hand, all rocks are typical I-type granitoids according to the A/CNK index (Fig. 7c and d), hence melts are interpreted to be juvenile, and reworking of Pre-Neoproterozoic crust can be excluded. An I-type granitoid suite is also indicated by Na_2O mostly > 3.2 wt.% (Chappel and White, 1974). The fractionation of these juvenile melts resulted in a trend from unfractionated I-types of group (I) towards A-type affinity of group (II) and group (III) according to the FeO/MgO versus $Zr + Nb + Ce + Y$ plot (Fig. 7e) of Whalen et al. (1987). Group (IV) samples cluster mostly in the field of fractionated felsic I-types (Fig. 7f). The geotectonic setting of the Sibai granitoids is constrained from Rb versus $Y + Nb$ diagrams of Pearce et al. (1984). Group (I) plots in the field of volcanic arc granitoids. All other groups show a trend towards within-plate granitoids which are characterised by higher Y and Nb concentrations (Fig. 7g and h). This classification is consistent with the trace element spidergrams (Fig. 8) normalised to ocean ridge granites (Pearce et al., 1984), Typical features of these patterns include enrichment of K, Rb and Th and low relative abundance from Ta to Yb. Group (II) and (III) granitoids have Hf to Y values close to the normalising values and high K, Rb and Th reflecting progressive fractionation. Small bodies of group (IV) are comparatively variable but generally display patterns similar to those of groups (II) and (III). These data are interpreted to represent an evolutionary trend from the island arc setting represented by group (I) to late orogenic A-type magmatics of group (II) and (III). We emphasise that generation of A-type melts is not limited to anorogenic settings. As documented by Whalen et al. (1987) those melts are frequently associated with late orogenic exhumation and strike slip tectonics; a scenario we favour to explain generation of group (II, III) granitoids. Scatter of the Late Tectonic Granites of group (IV) is interpreted to reflect remelting of various precursor rocks during a late stage of the evolution.

Fig. 7. Discrimination diagrams for the Sibai granitoids. Group (I), (II) and (III) in the first column give evidence for progressive fractionation of melts, whereas group (IV) in the second column exhibits significant scatter. (a) Quartz (Q)–alkalifeldspar (A)–plagioclase (P) triangle for group (I) to (III) and (b) for group (IV). (c) A/CNK index plots calculated from geochemical data for group (I) to (III) and (d) for group (IV) supporting the field observations that in the Sibai all granitoids are formed by juvenile melts, (e and f) $Zr + Nb + Ce + Y$ vs. FeO/MgO plot after Whalen et al. (1987). Note that group (II) and group (III) granitoids show a strong A-type affinity, whereas group I granitoids show an I-type characteristic, (g) Rb vs. $(Y + Nb)$ diagram for group (I) to (III) and (h) for group (IV) showing the tectonic fields after Pearce et al. (1984). Note the increasing within-plate component from group (I) to (III). The spread of group (IV) results from contamination of these comparatively small late tectonic units. Syn COLG, Syncollisional granite; WPG, Within-plate granite; VAG, Volcanic arc granite; ORG, Ocean ridge granite.

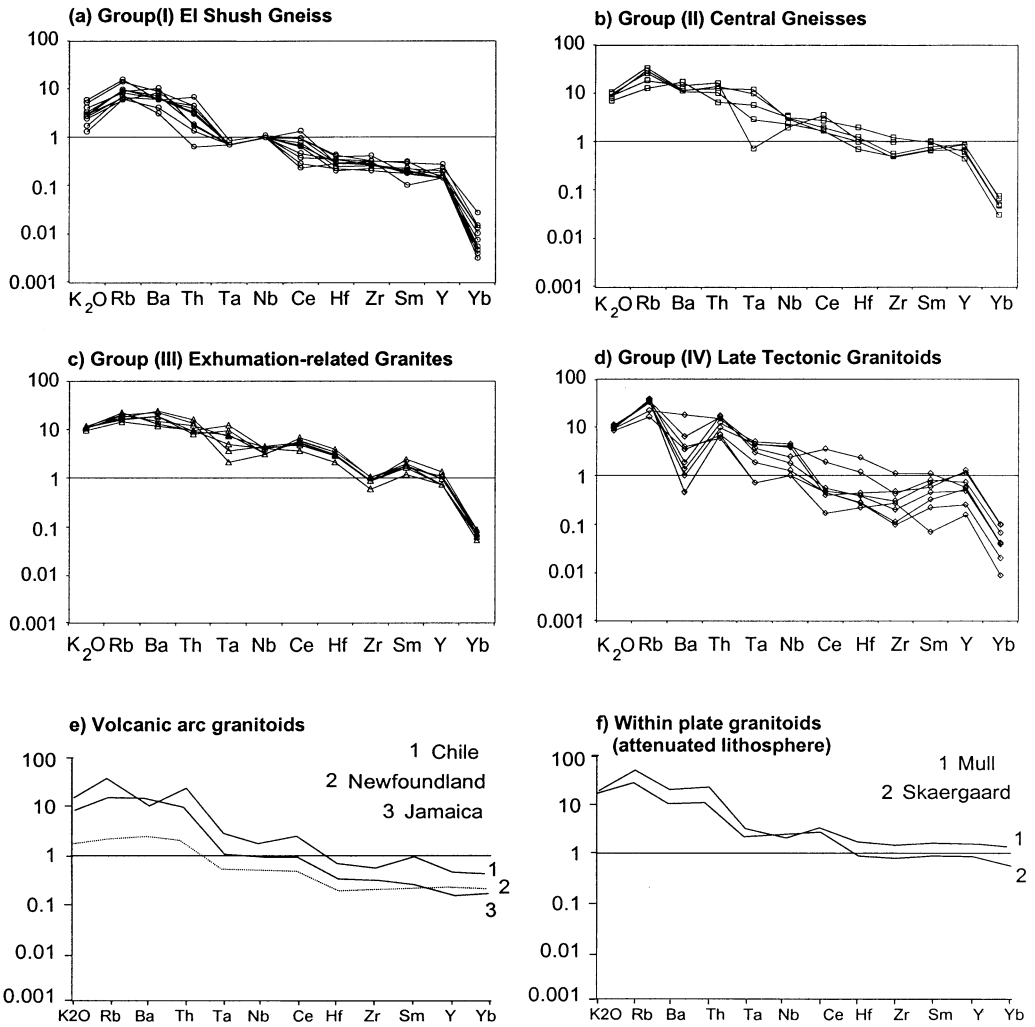

Fig. 8. Ocean ridge granite (ORG) normalised geochemical patterns for the Sibai granitoids (QRG normalisation values after Pearce et al. (1984). (a) Group (I) shows a characteristic volcanic arc pattern, whereas groups (II, b) and (III, c) progressively evolve towards a within-plate signature. Group (IV, d) shows a considerable spread due to variable contamination of the relatively small granitoid bodies. (e, f) Reference patter, for typical volcanic arc granitoids and within plate granitoids after Pearce et al. (1984). For further explanation see text.

6. Discussion

One aspect of this paper is to contribute to the discussion whether reworked pre-Neoproterozoic or juvenile Neoproterozoic crust is represented by the core complexes of the Eastern Desert. At least for the Sibai dome, where more than 90% of outcrop surface consists of granitoid rocks, we argue that these rocks formed during island arc accretion and orogen-parallel extension in the late Proterozoic. The granites have been variably deformed and evolved during different stages of oblique convergence, orogen-parallel extension and exhumation rather than during different orogenic cycles.

A second aspect involves kinematic and geodynamic processes during magma emplacement within the Central Eastern Desert of Egypt. The

East African Orogen along the eastern margin of Westgondwana formed by oblique island arc accretion in the Neoproterozoic, (e.g. Stern, 1994; Fritz et al., 1996). Plate convergence caused formation of nappes containing ophiolites and related supracrustal rocks accompanied by calc-alkaline magmatism. Within the Sibai area this stage is represented by the I-type suite of the El Shush Gneiss (group I granitoids) that intruded at approximately, 680 ± 10 Ma ago and had subsequently been incorporated into Neoproterozoic thrust tectonics (Fig. 9a). During oblique convergence thrusts propagated progressively to the western foreland thereby incorporating molasse sediments into the Neoproterozoic nappe assembly. Pronounced orogen-parallel extension was coevally active within internal portions of the orogen (Fritz et al., 1996; Fowler and Osman,

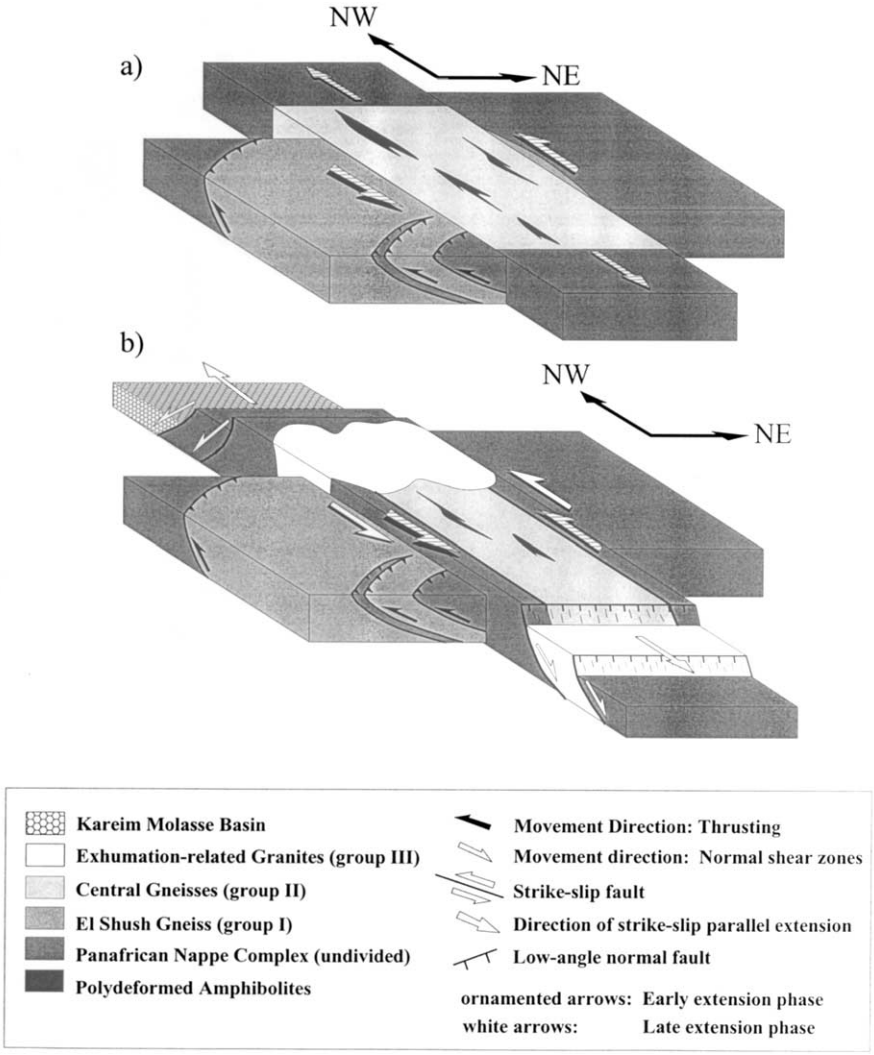

Fig. 9. Two stage model for the evolution of the Sibai magmatic core complex. (a) Formation of the sinistral wrench corridor associated with NE–SE directed extension and synkinematic intrusion of group (II) granitoids (central block). (b) Ongoing northwest–southeast directed extension triggered the intrusion of group (III) granitoids and the formation of detachment shear zones. Continuous activity of strike-slip and normal shear zones leads to the exhumation of the core complex and the formation of the Kareim molasse basin in the northwest.

2001) and was concentrated along the Najd Fault System. Deformation along the Najd Fault System partitioned into sets of sinistral strike-slip and normal shear zones bounding a number of metamorphic and/or magmatic core complexes. Granitoids of variable ages intruded this zone oforogcn-parallcl extension. The Sibai magmatic core complex consists mainly of such granitoids (group II, III granitoids) and the structures are related to this wrench tectonism. This interpretation is in contrast to that of Kamal El Din (1993) who interpreted all shear zones bounding the Sibai Core Complex as low-angle thrusts.

The geochemical signatures of the Sibai granitoids display progressive fractionation which corresponds to their age variations. The change from calc-alkaline to alkaline magmatism at Sibai occurred approximately at 650 Ma. Transition in tectonic and magmatic style from compressional to extensional setting at approximately 600 Ma has been already recognised by Stern and Hedge (1985), however, in the Sibai the transition occurred earlier. Orogen-parallel extension tectonics and the formation of the Najd Fault System commenced at approximately 650 Ma as suggested by the deformational overprint of group (II) rocks. The granitoids emplaced within this setting exhibit vertical foliations and horizontal lineations as result of distributed sinistral shear tectonics (Fig. 9a). Transpression tectonics (Sanderson and Marchini, 1984), which describes a specific three-dimensional geometry of a wrench zone between two obliquely converging blocks may result in this structural association. Depending on the angle of convergence between these converging blocks and the accumulated strain, vertical foliations and horizontal stretching lineations or vertical lineations occur. However, in a pure transpressional model horizontal stretching lineations are limited to low strains and/or very small convergence angles (Robin and Cruden, 1994; Teyssier et al., 1995). Translated to the scenario described in this paper, a very high component of shear parallel to the Najd Fault System would be required. It is more realistic to apply a model that combined transpression with lateral, Najd Fault parallel extrusion. Within combined transpression and shear zone parallel extrusion vertically foliated and horizontally stretched rocks typically occur over a wide range of convergence angles and strain intensities.

The geometry of this type of ductile deformation is characterised by vertical and lateral flow of material. Here, rise of magma follows vertical flow lines and is supported by horizontal driving forces (de Saint Blanquat et al., 1998). Combined transpression/extrusion may cause variable amount of crustal thickening or extension depending on the angle of plate convergence and rate of lateral extrusion (Tikoff and Teyssier, 1994). Neither significant exhumation nor topographic relief is necessarily associated with this process.

Group (III) granites which intruded shortly after those of group (II), display progressively evolving chemistry and differ significantly in tectonic style. Structural features associated with this stage of magmatism point to pronounced rock exhumation. Along the southern margins of Sibai this is documented by low-angle normal shear zones that are related to the emplacement of the Abu Markhat and Um Shaddad gneisses. To the north of Sibai this stage is characterised by tectonically and magmatically induced exhumation of rocks and the deposition of molasse-type sediments (Fritz and Messner, 2000). This indicates that a topographic relief had been established at this time (Fig. 9b).

Time brackets derived from single zircon ages document that production of volcanic arc granitoids and nappe stacking at Sibai continued at least until 680 Ma. At approximately 650 Ma, tectonics shifted towards a combination of transpression and shear zone parallel extrusion. We interpret the magmatism at Sibai as a result of one progressive, long term orogenic process. Such long term magmatic evolutions controlled by wrench tectonics have been reported from both, modern as well as ancient orogens (Ague and Brimhall, 1988; Bellier and Sebrier, 1994; de

Saint Blanquat et al., 1998; Tikoff and Teyssier, 1994; Fritz et al., 2002). We want to emphasise that the intrusion ages of granitoids may vary along the strike of the Najd Fault System reflecting northward propagation of tectonism (Beyth et al., 1994). The concentration of granitoids along the Najd wrench system suggests a magmatically active zone. Enhanced temperatures weakened the lithosphere and favoured extension parallel to the wrench corridor. On the other hand, extension itself supported the emplacement of granitoids. We argue that magmatically and tectonically induced extension are interrelated, auto-catalytic processes (de Saint Blanquat et al., 1998).

A third aspect of this paper concerns the formation of core complexes in general and the problem why core complexes in the Central Eastern Desert are aligned along the narrow Najd Fault System. Several mechanisms have been proposed to explain exhumation of core complexes within orogenic belts. These include processes related to instabilities induced by crustal thickening (crustal scale duplex formation, Johnson, 1994; gravitational collapse, Dewey, 1988; orogen-parallel unroofing, Neubauer et al., 1999) or processes related to general lithospheric or crustal extension, (e.g. Wernicke, 1985; Lister and Davis, 1989). Recently a scenarios for orogenic collapse has been described from extensional zones at Sinai (Blasband et al., 2000). The above-mentioned scenarios and also those described by Blasband et al. (2000) do not explain the exhumation of the Sibai. Neither significant crustal thickening nor bulk lithospheric extension is evident in the Central Eastern Desert (Burke and Sengör, 1986; Stern, 1994; Fritz et al., 1996, 2002). Instead, continuous magmatic activity coeval with wrench tectonism suggests that exhumation was closely related to magmatic activity. As described above, we consider magmatism and shear zone activity to be autocatalytic processes. This can explain the concentration of wrench tectonism and magmatism along the relatively narrow corridor of the Najd Fault System. Hence, the Sibai dome is best described as a magmatic core complex that evolved during transcurrent plate motion.

Acknowledgements

We acknowledge fruitful discussions with E. Wallbrecher, G. Hoinkes and J. Loizenbauer. A.A. Khudeir is thanked for introducing us into the Geology of Egypt. A previous version of the manuscript was significantly improved by K. Stüwe. Reviews and helpful suggestions by R.J. Stern (Dallas) and R.O. Greiling (Heidelberg) are gratefully acknowledged. This work has been supported by the Austrian Science Foundation (FWF Grants P09703-GEO and P12837-GEO).

References

Ague, R., Brimhall, G.H., 1988. Magmatic arc asymmetry and distribution of anomalous plutonic belts in the batholiths of California: effects of assimilation, crustal thickness, and depth of crystallisation. Geol. Soc. Am. Bull. 100, 912–927.

Al Shanti, A.M., Gass, I.G., 1983. The upper Proterozioc ophiolite melange zones of the easternmost Arabian-Nubian Shield. J. Geol. Soc. London 140, 867–876.

Bellier, O., Sebrier, M., 1994. Relationship between tectonism and volcanism along the Great Sumatran Fault Zone deduced by SPOT image analyses. Tectonophysics 233, 215–231.

Beyth, M., Stern, R.J., Altherr, R., Kröner, A., 1994. The late Precambrian Timna igneous complex, Southern Israel: Evidence for comagmatic-type sanukitoid monzodiorite and alkali granite magma. Lithos 31, 103–124.

Blasband, B., Brooijmans, P., Dirks, P., Visser, W., White, S., 1997. A Pan-African core complex in the Sinai, Egypt. Geologie Mijnbouw 76, 247–266.

Blasband, B., White, S., Brooijmans, P., De Boorder, H., Visser, W., 2000. Late proterozoic extensional collapse in the Arabian-Nubian Shield. J. Geol. Soc. London 157, 615–628.

Bregar, M., 1996. Exhumation history of the Gebel Sibai Dome (Eastern Desert of Egypt): constraints from evolution of low-angle normal faults and corresponding footwall units. M.Sc. thesis, Univ. of Graz, Austria (unpublished).

Bregar, M., Fritz, H., Unzog, W., 1996. Structural evolution of low-angle normal faults SE of the Gebel El Sibai Crystalline Dome; Eastern Desert, Egypt: evidence from paleopiezometry and vorticity analysis. Zbl. Geol. Paläont 3/4, 243–256.

Burke, K, Sengör, C., 1986. Tectonic escape in the evolution of the continental crust. In: Barazangi, M. (Ed.), Reflection Seismology: the continental crust. American Geophysical Union Geodynamic Series, vol. 14. pp. 41–53.

Chappel, B.W., White, A.J.R., 1974. Two contrasting granite types. Pacific Geol. 8, 173–174.

Debon, F., Le Fort, P., 1983. A chemical–mineralogical classification of common plutonic rocks and associations. Trans. R. Soc. Edin.: Earth Sci. 73, 135–149.

de Saint Blanquat, M., Tikoff, B., Teyssier, C., Vigneresse, J.-L., 1998. Transpressional kinematics and magmatic arcs. In: Holdsworth, R.E., Strachan, R.A., Dewey, J.F. (Eds.), Continental Transpression and Transtension Tectonics, vol. 135. Geological Society of London, pp. 327–340 Special Publications.

Dewey, J.F., 1988. Extensional collapse of orogens. Tectonics 7, 1123–1139.

El Gaby, S., El Nady, O., Khudeir, A.A., 1984. Tectonic evolution of the basement complex in the central Eastern Desert. Geologische Rundschau 73, 1019–1036.

El Gaby, S., List, F.K., Tehrani, R., 1990. The basement complex of the Eastern Desert and Sinai. In: Said, R. (Ed.), The Geology of Egypt. Balkema, Rotterdam, pp. 175–184.

El Gaby, S., Khudeir, A.A., Abdel Tawab, M., Atalia, R.F., 1991. The metamorphosed volcano-sedimentary succession of Wadi Kid, southeastern Sinai, Egypt. Ann. Geol. Surv. Egypt 17, 19–35.

El Ramly, M.F., Greiling, R.O., Rashwan, A.A., Rasmy, A.H., 1993. Explanatory note to accompany the geological and structural maps of Wadi Hafafit area, Eastern Desert of Egypt. Geol. Surv. Egypt Paper 68, 1–53.

Fowler, T.J., Osman, A.F., 2001. Gneiss-cored interference dome associated with two phases of late Pan-African thrusting in the central Eastern Desert, Egypt. Precambrian Res. 108, 7–43.

Fritz, H., Messner, M., 2000. Intramontane basin formation during oblique convergence in the Eastern Desert of Egypt; magmatically versus technically induced subsidence. Tectonophysics 315, 143–160.

Fritz, H., Wallbrecher, E., Khudeir, A.A., Abu El Ela, F., Dallmeyer, R.D., 1996. Formation of Neoproterozoic metamorphic core complexes during oblique convergence (Eastern Desert, Egypt). J. African Earth Sci. 23, 311–329.

Fritz, H., Dallmeyer, R.D., Wallbrecher, E., Loizenbauer, J., Hoinkes, G., Neumayr, P., Khudeir, A.A., 2002. Neoproterozoic tectonothermal evolution of the central Eastern Desert of Egypt: a slow velocity tectonic process of core complex exhumation. J. African Earth Sci. 34, 137–155.

Garfunkel, Z., 1988. Relation between continental rifting and uplifting: evidence from the Suez rift and the northern Red Sea. Tectonophysics 150, 33–49.

Gass, I.G., 1982. Upper Proterozoic (Pan-African) calc-alkaline magmatism in northeastern Africa and Arabia. In: Thorpe, R.S. (Ed.), Andesites. Wiley, New York, pp. 591–609.

Greenberg, J.K., 1981. Characteristics and origin of Egyptian Younger Granites: summary. Geol. Soc. Am. Bull. 92, 224–232.

Greiling, R.O., Rashwan, A.A., El Ramly, M.F., Kamal El Din, G.M., 1993. Towards a comprehensive structural synthesis of the (Proterozoic) Arabian-Nubian Shield in E. Egypt. In: Thorweihe, U., Schandelmcier, H. (Eds.), Geoscientific Research in Northeast Africa. Balkema, Rotterdam, pp. 15–19.

Greiling, R.O., Abdeen, M.M., Dardir, A.A., Akhal, H., El Ramly, M.F., Kamal El Din, G.M., Osman, A.F., Rashwan, A.A., Rice, A.H.N., Sadek, M.F., 1994. A structural synthesis of the Proterozoic Arabian-Nubian Shield in Egypt. Geologische Rundschau 83, 484–501.

Grothaus, B.D., Eppler, D., Ehrlich, R., 1979. Depositional environment and structural implications of the Hammamat Formation, Egypt. Ann. Geol. Surv. Egypt 9, 564–590.

Habib, M.S., Ahmed, A.A., El Nady, O.M., 1985. Two orogenies in the Meatiq area of the CED, Egypt. Precambrian Res. 30, 83–111.

Hashad, A.H., Sayyah, T.A., El Kholy, S.B., Youssef, A., 1972. Rb/Sr isotopic age determinations of some basement Egyptian granites. Egypt. J. Geol. 27, 73–92.

Hassan, M.A., Hashad, A.H., 1990. Precambrian of Egypt. In: Said, R. (Ed.), The Geology of Egypt. Balkema, Rotterdam, pp. 201–248.

Hawkesworth, C., Turner, S., Gallagher, K., Hunter, A., Bradshaw, T., Rogers, N., 1995. Calc-alkaline magmatism, lithospheric thinning and extension in the Basin and Range. J. Geophys. Res. 100, 10271–10286.

Hill, E.J., Baldwin, S.L., Lister, G.S., 1995. Magmatism as an essential driving force for formation of active metamorphic core complexes in eastern Papua New Guinea. J. Geophys. Res. 100, 10441–10451.

Hume, W.F., 1934. The fundamental Precambrian rocks of Egypt and the Sudan. In: Geology of Egypt, vol. 2, Geol. Surv. Egypt, p. 300.

Johnson, M.R.W., 1994. Culminations and denial uplifts in the Himalaya. Tectonophysics 239, 139–147.

Kamal El Din, G.M., 1993. Geochemistry and tectonic significance of the Pan-African El Sibai window, Central Eastern Desert, Egypt. Scientific Series of the International Bureau, 19, Forschungszentrum Jüilich, p. 154.

Khudeir, A.A., El Gaby, S., Greiling, R.O., Kamal El Din, G.M., 1992. Geochemistry and tectonic significance of polymetamorphosed amphibolites in the Gebel Sibai window, Central Eastern Desert, Egypt. In: Geology of the Arab World. Cairo University, pp. 461–476.

Khudeir, A.A., El Gaby, S., Kamal El Din, G.M., Asran, A.M.H., Greiling, R.O., 1995. The pre-Pan-African deformed granite cycle of the Gabal El Sibai swell, Eastern Desert, Egypt. J. African Earth Sci. 21, 395–406.

Klötzli, U.S., 1997. Zircon evaporation; TIMS method and procedures. Analyst 122, 1239–1248.

Klölzli, U.S., 1999. Th/U zonation in zircon derived from evaporation analysis: a model and its implications. Chem. Geol. 158, 325–333.

Klötzli, U.S., Parrish, R.R., 1996. Zircon U–Pb and Pb–Pb geochronology of the Rastenberg granodiorite, South Bohemian Massif, Austria. Miner. Petrol. 58, 197–214.

Kober, B., 1987. Single-zircon evaporation combined with Pb^{+} emitter bedding for $^{207}Pb/^{206}Pb$-age investigations using thermal ion mass spectromctry and implications to zirconology. Contrib. Miner. Petrol. 96, 63–71.

Kröner, A., 1985. Ophiolites and the evolution of tectonic boundaries in the late Proterozoic Arabian-Nubian Shield of Northeast Africa and Arabia. Precambrian Res. 27, 277–300.

Kröner, A., Eyal, M., Eyal, Y., 1990. Early Pan-African evolution of the basement around Elat, Israel, and the Sinai Peninsula revealed by single zircon evaporation dating, and implications for crustal accretion rates. Geology 18, 545–548.

Kröner, A., Todt, W., Hussein, I.M., Mansour, M., Rashwan, A.A., 1992. Dating of late Proterozoic ophiolites in Egypt and the Sudan using the single grain zircon evaporation technique. Precambrian Res. 59, 15–32.

Kröner, A., Krüger, J., Rashwan, A.A., 1994. Age and tectonic setting of granitoid gneisses in the Eastern Desert of Egypt and south-west Sinai. Geologische Rundschau 83, 502–513.

Lister, G.S., Davis, G.A., 1989. The origin of metamorphic core complexes and detachment faults formed during continental extension in the northern Colorado River region, USA. J. Struct. Geol. 11, 65–94.

Loizenbauer, L., Wallbrecher, E., Fritz, H., Neumayr, P., Khudeir, A.A., Kloetzli, U., 2001. Structural Geology, single zircon ages and fluid inclusion studies of the Meatiq metamorphic core complex: Implications for Neoproterozoic tectonics in the Eastern Desert of Egypt. Precambrian Res. 110, 357–383.

Ludwig, K.R., 1992. Isoplot: a plotting and regression program for radiogenic-isotope data, version 2.57. United States Geological Survey, Open-file report, 91–445.

Messner, M., Fritz, H., Pelz, K., Unzog, W., 1996. Beckenbildung in vcrschiedenen tektonischen Settings: Strukturelle Rahmen und Abbildung der Tektonik in der Sedimentation. Symposium Tektonik, Strukturgeologie, Kristallingeologie, 6, Facultas Verlag, Salzburg, pp. 275–278.

Neubauer, F., Genser, J., Kurtz, W., Wang, X., 1999. Exhumation of the Tauern window, Eastern Alps. Phys. Chem. Earth 24, 675–680.

Neumayr, P., Hoinkes, G., Puhl, J., 1995. Constraints on the P–T–t evolution of a polymetamorphic Panafrican basement dome in the Central Eastern Desert (Egypt). Terra Abstracts 7, 316.

Neumayr, P., Hoinkes, G., Puhl, J., Mogessie, A., Khudeir, A.A., 1998. The Meatiq dome (Eastern Desert, Egypt) a Precambrian metamorphic core complex: petrological and geological evidence. J. Metamorphic Geol. 16, 259–279.

O'Connor, E.A., Bennett, J.D., Rashwan, A.A., Nasr, B.B., Mansour, M.M., Romani, R.F., Sadek, M.F., 1994. Crustal growth in the Nubian Shield of Southeastern Egypt, Proceedings International Conference 30 years cooperation in annals of the Geological Survey of Egypt, Cairo, pp. 189–195.

Omar, G.I., Steckler, M.S., Buck, W.R., Kohn, B.P., 1989. Fission track analysis of basement apatites at the western margin of the Gulf of Suez rift, Egypt; evidence for synchronicity of uplift and subsidence. Earth Planetary Sci. Lett. 94, 316–328.

Pearce, J.A., Harris, N.B.W., Tindle, A.G., 1984. Trace element discrimination diagrams for the tectonic interpretation of granitic rocks. J. Petrol. 25, 956–983.

Rashwan, A.A., 1991. Petrography, Geochemistry and Petrogenesis of the Migif-Hafafit Gneisses at Hafafit Mine Area, Egypt, Scientific Series of the International Bureau, 5, Forschungszentrum Jülich, pp. 359.

Rice, A.H.N., Sadek, M.F., Rashwan, A.A., 1993. Igneous and structural relations in the Pan-African Hammamat Group, Igla Basin, Egypt. In: Thorwcihe, U., Schandelmeier, H. (Eds.), Geoscientific Research in Northeast Africa. Proceedings of the International Conference on Geoscientific Research in Northeast Africa. Balkema, Rotterdam, pp. 35–39.

Ries, A.C., Shaekleton, R.M., Graham, R.H., Fitches, W.R., 1983. Pan-African structures, ophiolites and melange in the Eastern Desert of Egypt; a traverse at 26 degrees N. J. Geol. Soc. London 140, 75–95.

Robin, P.-Y.F., Cruden, A.R., 1994. Strain and vorticity patterns in ideal transpression zones. J. Struct. Geol. 16, 447–466 Abstract.

Sanderson, D.J., Marchini, W.R.D., 1984. Transpression. J. Struct. Geol. 6, 449–458.

Shackleton, R.M., Ries, A.C., Graham, R.H., Fitches, W.R., 1980. Late Precambrian ophiolite melange in the Eastern Desert of Egypt. Nature 285, 472–474.

Shand, S.J., 1927. Eruptive rocks. Their genesis, composition, classification and their relation to ore-deposits, Murby, London.

Stern, R.J., 1985. The Najd Fault System, Saudi Arabia and Egypt: a late Precambrian rift-related transform system. Tectonics 4, 497–511.

Stern, R.J., 1994. Arc assembly and continental collision in the Neoproterozoic East African Orogen: implications for the consolidation of Gondwanaland. Annu. Rev. Earth Planet Sci. 22, 319–351.

Stern, R.J., Hedge, C.E., 1985. Geochronologic and isotopic constraints on late Precambrian crustal evolution in the Eastern Desert of Egypt. Am. J. Sci. 285, 97–172.

Stern, R.J., Manton, W.I., 1987. Age of Feiran basement rocks, Sinai: implications for late Precambrian crustal evolution in the northern Arabian-Nubian Shield. J. Geol. Soc. London 144, 569–575.

Stern, R.L., Kröner, A., Rashwan, A.A., 1991. A late Precambrian ($\sim$710 Ma) high volcanicity rift in the southern Eastern Desert of Egypt. Geologische Rundschau 80, 155–170.

Sturchio, N.C., Sultan, M., Batiza, R., 1983. Geology and origin of Meatiq dome, Egypt: a Precambrian metamorphic core complex. Geology 11, 72–76.

Tikoff, B., Teyssier, C., 1994. Strain modeling of displacement-field partitioning in transpressional orogens. J. Struct. Geol. 16, 1575–1588.

Teyssier, C., Tikoff, B., Markley, M., 1995. Oblique plate motion and continental tectonics. Geology 23, 447–450.

Unzog, W., Kurz, W., 2000. Progressive development of lattice preferred orientations (LPOs) of naturally deformed quartz within a transpressional collision zone (Panafrican Orogen in the Eastern Desert of Egypt). J. Struct. Geol. 22, 1827–1835.

Wallbrecher, E., Fritz, H., Khudeir, A.A., Abu El Ela, F., 1993a. Displacement partitioning and formation of metamorphic domes due to oblique collision: the Panafrican orogeny in Egypt. Terra Abstracts 5, 249.

Wallbrecher, E., Fritz, H., Khudeir, A.A., Farahad, F., 1993b. Kinematics of Pan-African thrusting and extension in Egypt. In: Thorweihe, U., Schandelmeier, H. (Eds.), Geoscientific research in Northeast Africa. Proceedings of the International Conference on Geoscientific Research in Northeast Africa. Balkema, Rotterdam, pp. 27–30.

Wernicke, B., 1985. Uniform-sense normal simple shear of continental lithosphere. Can. J. Earth Sci. 22, 108–125.

Whalen, J.B., Kenneth, L.C., Chappell, B.W., 1987. A-type granites: geochemical characteristics, discrimination and petrogenesis. Contrib. Miner. Petrol. 95, 407–419.

Willis, K.M., Stern, R.J., Clauer, N., 1988. Age and geochemistry of late Precambrian sediments of the Hammamat series from the Northeastern Desert of Egypt. Precambrian Res. 42, 173–187.